Eur. Phys. J. C (2017) 77:81
DOI 10.1140/epjc/s10052-017-4645-8

THE EUROPEAN PHYSICAL JOURNAL C

Regular Article - Theoretical Physics

Equation of state, universal profiles, scaling and macroscopic quantum effects in warm dark matter galaxies

H. J. de Vega[1], **N. G. Sanchez**[2,a]

[1] LPTHE CNRS UMR 7589, Sorbonne Universités, Université Pierre et Marie Curie UPMC Paris VI, Tour 24, 5ème. étage, Boite 126, 4, Place Jussieu, 75252 Paris Cedex 05, France

[2] Observatoire de Paris, LERMA CNRS UMR 8112, Observatoire de Paris PSL Research University, Sorbonne Universités UPMC Paris VI, 61, Avenue de l'Observatoire, 75014 Paris, France

Received: 22 December 2016 / Accepted: 24 January 2017 / Published online: 8 February 2017

Abstract The Thomas–Fermi approach to galaxy structure determines self-consistently and non-linearly the gravitational potential of the fermionic warm dark matter (WDM) particles given their quantum distribution function $f(E)$. This semiclassical framework accounts for the quantum nature and high number of DM particles, properly describing gravitational bounded and quantum macroscopic systems as neutron stars, white dwarfs and WDM galaxies. We express the main galaxy magnitudes as the halo radius r_h, mass M_h, velocity dispersion and phase space density in terms of the surface density which is important to confront to observations. From these expressions we **derive** the general equation of state for galaxies, i.e., the relation between pressure and density, and provide its analytic expression. Two regimes clearly show up: (1) Large diluted galaxies for $M_h \gtrsim 2.3 \times 10^6\ M_\odot$ and effective temperatures $T_0 > 0.017$ K described by the classical self-gravitating WDM Boltzman gas with a space-dependent perfect gas equation of state, and (2) Compact dwarf galaxies for $1.6 \times 10^6\ M_\odot \gtrsim M_h \gtrsim M_{h,\min} \simeq 3.10 \times 10^4\ (2\,\mathrm{keV}/m)^{\frac{16}{5}}\ M_\odot$, $T_0 < 0.011$ K described by the quantum fermionic WDM regime with a steeper equation of state close to the degenerate state. In particular, the $T_0 = 0$ degenerate or extreme quantum limit yields the most compact and smallest galaxy. In the diluted regime, the halo radius r_h, the squared velocity $v^2(r_h)$ and the temperature T_0 turn to exhibit square-root of M_h **scaling** laws. The normalized density profiles $\rho(r)/\rho(0)$ and the normalized velocity profiles $v^2(r)/v^2(0)$ are **universal** functions of r/r_h reflecting the WDM perfect gas behavior in this regime. These theoretical results contrasted to robust and independent sets of galaxy data remarkably reproduce the observations. For the small galaxies, $10^6 \gtrsim M_h \geq M_{h,\min}$, the equation of state is galaxy mass dependent and the density and velocity profiles are not anymore universal, accounting to the quantum physics of the self-gravitating WDM fermions in the compact regime (near, but not at, the degenerate state). It would be extremely interesting to dispose of dwarf galaxy observations which could check these quantum effects.

Contents

1 Introduction

Dark matter (DM) is the main component of galaxies: the fraction of DM over the total galaxy mass goes from 95% for large diluted galaxies till 99.99% for dwarf compact galaxies. Therefore, DM alone should explain the main structure of galaxies. Baryons should only give corrections to the pure DM results.

Warm dark matter (WDM), that is, dark matter formed by particles with masses in the keV scale receives increasing attention today ([1–10] and references therein).

At intermediate scales ∼100 kpc, WDM gives the **correct abundance** of substructures and therefore WDM solves the cold dark matter (CDM) overabundance of structures at small

[a] e-mail: Norma.Sanchez@obspm.fr

scales [11–19]. For scales larger than 100 kpc, WDM yields the same results than CDM. Hence, WDM agrees with all the observations: small scale as well as large scale structure observations and CMB anisotropy observations.

Astronomical observations show that the DM galaxy density profiles are **cored** till scales below the kpc [20–25]. On the other hand, N-body CDM simulations exhibit cusped density profiles with a typical $1/r$ behavior near the galaxy center $r = 0$. Inside galaxy cores, below ∼100 pc, N-body classical physics simulations do not provide the correct structures for WDM because quantum effects are important in WDM at these scales. Classical physics N-body WDM simulations exhibit cusps or small cores with sizes smaller than the observed cores [26–29]. WDM predicts correct structures and cores with the right sizes for small scales (below kpc) when the **quantum** nature of the WDM particles is taken into account [30,31]. This approach is **independent** of any WDM particle physics model.

We follow here the Thomas–Fermi approach to galaxy structure for self-gravitating fermionic WDM [30,31]. This approach is especially appropriate to take into account quantum properties of systems with large number of particles. That is, macroscopic quantum systems as neutron stars and white dwarfs [32,33]. In this approach, the central quantity to derive is the DM chemical potential $\mu(\mathbf{r})$, which is the free energy per particle. For self-gravitating systems, the potential $\mu(\mathbf{r})$ is proportional to the gravitational potential $\phi(\mathbf{r})$, $\mu(\mathbf{r}) = \mu_0 - m\,\phi(\mathbf{r})$, μ_0 being a constant, and it obeys the **self-consistent** and **non-linear** Poisson equation,

$$\nabla^2\mu(\mathbf{r}) = -4\,\pi\,g\,G\,m^2\int\frac{d^3p}{(2\,\pi\,\hbar)^3}\,f\left(\frac{p^2}{2\,m}-\mu(\mathbf{r})\right). \tag{1.1}$$

Here G is Newton's gravitational constant, g is the number of internal degrees of freedom of the DM particle, p is the DM particle momentum and $f(E)$ is the energy distribution function. This is a semiclassical gravitational approach to determine self-consistently the gravitational potential of the quantum fermionic WDM given its distribution function $f(E)$.

The terminology "Thomas–Fermi approach" is used here by analogy with the effective quantum mechanical treatement implying a quantum statistical distribution function. Notice, however, that the Thomas–Fermi method in atomic physics does not lead to an integro-differential equation but rather to a non-linear differential equation.

In the Thomas–Fermi approach, DM dominated galaxies are considered in a stationary state. This is a realistic situation for the late stages of structure formation since the free-fall (Jeans) time t_{ff} for galaxies is much shorter than the age of galaxies. t_{ff} is at least one or two orders of magnitude smaller than the age of the galaxy.

We consider spherical symmetric configurations where Eq. (1.1) becomes an ordinary non-linear differential equation that determines self-consistently the chemical potential $\mu(r)$ and constitutes the Thomas–Fermi approach [30,31] (see also Refs. [34–36]). We choose for the energy distribution function a Fermi–Dirac distribution

$$f(E) = \frac{1}{\mathrm{e}^{E/T_0}+1},$$

where T_0 is the characteristic one-particle energy scale. T_0 plays the role of an effective temperature scale and depends on the galaxy mass. The Fermi–Dirac distribution function is justified in the inner regions of the galaxy, inside the halo radius where we find that the Thomas–Fermi density profiles perfectly agree with the observations.

The collisionless self-gravitating gas is an isolated system which is not integrable. Therefore, it is an ergodic system that can thermalize [37]. Namely, the particle trajectories explore ergodically the constant energy manifold in phase-space, covering it uniformly according to precisely the micro-canonical measure and yielding to a thermal situation [37].

Physically, these phenomena are clearly understood because in the inner halo region $r \lesssim r_h$, the density is higher than beyond the halo radius. The gravitational interaction in the inner region is strong enough and thermalizes the self-gravitating gas of DM particles while beyond the halo radius the particles are too dilute to thermalize, namely, although they are virialized, they had not enough time to accomplish thermalization. Notice that virialization always starts before than thermalization.

The solutions of the Thomas–Fermi equations (1.1) are characterized by the value of the chemical potential at the origin $\mu(0)$. Large positive values of $\mu(0)$ correspond to dwarf compact galaxies (fermions near the quantum degenerate limit), while large negative values of $\mu(0)$ yield large and diluted galaxies (classical Boltzmann regime).

Approaching the classical diluted limit yields larger and larger halo radii, galaxy masses and velocity dispersions. On the contrary, in the quantum degenerate limit we get solutions of the Thomas–Fermi equations corresponding to the **minimal** halo radii, galaxy masses and velocity dispersions.

The surface density

$$\Sigma_0 \equiv r_h\,\rho_0 \simeq 120\,M_\odot/\mathrm{pc}^2 \quad \text{up to } 10-20\%, \tag{1.2}$$

whete r_h stand for the halo radius and ρ_0 for the density at the center has the remarkable property of being nearly **constant** and independent of luminosity in different galactic systems (spirals, dwarf irregular and spheroidals, elliptics) spanning over 14 magnitudes in luminosity and over different Hubble types [38,39]. It is therefore a useful characteristic scale to express galaxy magnitudes.

Our theoretical results follow by solving the self-consistent and non-linear Poisson equation (1.1) which is **solely** derived from the purely **gravitational** interaction of the WDM particles and their **fermionic** nature.

The main galaxy magnitudes as the halo radius r_h, mass M_h, velocity dispersion and phase space density are analytically obtained and expressed in terms of the surface density, which is particularly appropriate to confront to observations over the whole range of galaxies.

In this paper we **derive** and analyze the general equation of state of galaxies which clearly exhibits two regimes: (1) large diluted galaxies for

$$M_h \gtrsim 3.7\ 10^6\ M_\odot, \quad \nu_0 \equiv [\mu(0)/T_0] < -5, \quad T_0 > 0.017\ \text{K}, \tag{1.3}$$

described by the classical WDM Boltzmann regime, and (2) compact dwarf galaxies for

$$1.6\ 10^6 \gtrsim M_h \geq M_{h,\min} \simeq 3.10\ 10^4 \left(\frac{2\,\text{keV}}{m}\right)^{\frac{16}{5}} M_\odot, \quad \nu_0 > -4,$$
$$T_0 < 0.011\ \text{K}, \quad 133 \left(\frac{2\,\text{keV}}{m}\right)^{\frac{8}{5}} \text{pc} \gtrsim r_h^{\min} \gtrsim 11.4 \left(\frac{2\,\text{keV}}{m}\right)^{\frac{8}{5}} \text{pc}, \tag{1.4}$$

described by the quantum fermionic regime close to the degenerate state.

In particular, the $T_0 = 0$ degenerate or extreme quantum limit yields the most compact and smallest galaxy: with minimal mass $M_{h,\min}$ and minimal radius, and maximal phase space density.

In Ref. [30] careful estimates of the halo mass and radius for the degenerate WDM self-gravitating gas were reported. For clarity, we reproduce and update the estimates here.

For an order-of-magnitude estimate, let us consider a halo of mass M_h and radius r_h of fermionic matter. Each fermion can be considered inside a cell of size $\Delta x \sim 1/n^{\frac{1}{3}}$ and therefore has a momentum

$$p \sim \frac{\hbar}{\Delta x} \sim \hbar\, n^{\frac{1}{3}}. \tag{1.5}$$

The associated quantum pressure P_q (flux of the momentum) has the value

$$P_q = n\ \sigma\ p \sim \hbar\ \sigma\ n^{\frac{4}{3}} = \frac{\hbar^2}{m}\, n^{\frac{5}{3}}, \tag{1.6}$$

where σ is the mean velocity given by

$$\sigma = \frac{p}{m} = \frac{\hbar}{m}\, n^{\frac{1}{3}}.$$

The system will be in dynamical equilibrium if this quantum pressure is balanced by the gravitational pressure,

$$P_G = \text{gravitational force/area} = \frac{G\ M_h^2}{r_h^2} \times \frac{1}{4\,\pi\ r_h^2}. \tag{1.7}$$

We estimate the number density as

$$n = \frac{M_h}{\frac{4}{3}\ \pi\ r_h^3\ m},$$

and we use $p = m\ \sigma$ to obtain from Eq. (1.6)

$$P_q = \frac{\hbar^2}{m\ r_h^5} \left(\frac{3\ M_h}{4\ \pi\ m}\right)^{\frac{5}{3}}. \tag{1.8}$$

Equating $P_q = P_G$ from Eqs. (1.7), (1.8) yields the following relations between the size r_h and the velocity σ with the mass M_h of the system:

$$r_h = \frac{3^{\frac{5}{3}}}{(4\,\pi)^{\frac{2}{3}}} \frac{\hbar^2}{G\ m^{\frac{8}{3}}\ M_h^{\frac{1}{3}}}$$
$$= 7.8\ \text{pc} \left(\frac{10^4\ M_\odot}{M_h}\right)^{\frac{1}{3}} \left(\frac{2\ \text{keV}}{m}\right)^{\frac{8}{3}} \tag{1.9}$$

$$v = \sqrt{3}\ \sigma = \sqrt{3} \left(\frac{4\,\pi}{81}\right)^{\frac{1}{3}} \frac{G}{\hbar}\ m^{\frac{4}{3}}\ M_h^{\frac{2}{3}}$$
$$= 4.64\ \frac{\text{km}}{\text{s}} \left(\frac{m}{2\ \text{keV}}\right)^{\frac{4}{3}} \left(\frac{M_h}{10^4\ M_\odot}\right)^{\frac{2}{3}}. \tag{1.10}$$

These estimates are in agreement with the precise Thomas–Fermi results in the degenerate limit [see Eq. (1.4)].

One may wonder whether these WDM configurations could decrease their size r_h increasing indefinitely their mass M_h and velocity σ. We derive from Eq. (1.9) the estimation for the velocity

$$v = \frac{3^{\frac{5}{2}}}{4\,\pi} \frac{1}{G\ m^4\ r_h^2} = 0.4726\ 10^{-3} \left(\frac{\text{pc}}{r_h}\right)^2 \left(\frac{2\ \text{keV}}{m}\right)^2. \tag{1.11}$$

For $r_h < 0.02$ pc the velocity reaches the speed of light and the non-relativistic estimates Eqs. (1.6), (1.9) and (1.11) are no more valid.

Let us estimate the quantum pressure P_q for ultrarelativistic particles, that is, $\sigma = 1/\sqrt{3}$. We have from Eqs. (1.5) and (1.6)

$$P_q = n\ \sigma\ p \sim \hbar\ \frac{1}{\sqrt{3}}\ n^{\frac{4}{3}} = \frac{1}{\sqrt{3}} \left(\frac{3\ M_h}{4\ \pi\ m}\right)^{\frac{4}{3}} \frac{1}{r_h^4}. \tag{1.12}$$

Equating $P_q = P_G$ from Eqs. (1.7)–(1.12) the factor $1/r_h^4$ cancels out and we find a fixed constant value for the mass M_h:

$$M_h^{\max} = \frac{3^{\frac{5}{4}}}{2\sqrt{\pi}} \frac{1}{G^{\frac{3}{2}} m^2} = 0.45432\ 10^{12}\ M_\odot \left(\frac{2\ \text{keV}}{m}\right)^2, \quad \text{ultrarelativistic particles.} \tag{1.13}$$

Namely, for decreasing r_h the mass M_h increases till a **stable configuration of maximal** mass value $M_h^{\max}$.

It must be noticed that the estimation Eq. (1.13) only differs by a factor three from the exact ultrarelativistic Thomas–Fermi result in the degenerate limit

$$M_h^{\max,\ \text{Thomas}-\text{Fermi}} = 1.2636\ 10^{12}\ M_\odot \left(\frac{2\ \text{keV}}{m}\right)^2, \quad \text{ultrarelativistic particles.} \tag{1.14}$$

The Chandrasekhar mass limit [32,33] for neutron stars formed by a degenerate gas of neutrons is analogous to the maximal mass Eqs. (1.13), (1.14) for self-gravitating degenerate WDM particles. Notice that strong interactions in neutron stars introduce corrections [32,33] to the self-gravitating degenerate gas of neutrons while the particle physics interactions of WDM are so weak that can be **safely** neglected.

It is useful the comparison with the estimations Eqs. (1.9), (1.10) for non-relativistic particles which imply

$$M_h = \frac{3^5}{(4\pi)^2} \frac{\hbar^6}{G^3 m^8 r_h^3} = 10^4\ M_\odot \left(\frac{7.8\ \text{pc}}{r_h^2}\right)^3 \left(\frac{2\ \text{keV}}{m}\right)^8, \tag{1.15}$$

$$M_h = \frac{3^{\frac{5}{4}}}{\sqrt{4\pi}} \frac{\hbar^{\frac{3}{2}}}{G^{\frac{3}{2}} m^2} v^{\frac{3}{2}} = 10^4\ M_\odot \left(\frac{v}{4.64\ \frac{\text{km}}{\text{s}}}\right)^{\frac{3}{2}} \left(\frac{2\ \text{keV}}{m}\right)^2. \tag{1.16}$$

For typical observed values of r_h and v, the values for M_h predicted by this non-relativistic estimation provide minimal values for M_h while if the WDM particles become ultrarelativistic we obtain the maximum possible value for M_h Eqs. (1.13), (1.14).

We thus have a whole range of stable WDM configurations ranging from a minimal M_h for non-relativistic WDM particles as in Eqs. (1.15), (1.16) till the maximal mass $M_h^{\max}$ in the ultrarelativistic limit as given by Eqs. (1.13), (1.14).

In fact, observations show that WDM particles are always non-relativistic and therefore galaxies with high masses near $M_h^{\max} \sim 10^{12}\ M_\odot$ in the degenerate ultrarelativistic regime Eqs. (1.13), (1.14) are not observed. On the contrary, the WDM non-relativistic estimates Eqs. (1.9), (1.10) and (1.15), (1.16) are **observationally realistic** for ultracompact galaxies.

As we see below in Sect. 2, observations show that real galaxies in their whole range of masses, sizes and velocities turn to be non-degenerate (non-zero temperature) solutions of the Thomas–Fermi equations and in particular the ultracompact galaxies are close to the zero temperature degenerate state.

A dwarf galaxy with a halo mass $M_h \simeq 10^6\ M_\odot$ arises as a solution of the Thomas–Fermi approach near the quantum degenerate regime. We obtain for a halo mass $M_h \simeq 10^6\ M_\odot$ a halo radius $r_h \simeq 100$ pc as one can see from Fig. 2 and a galaxy temperature $T_0 \simeq 0.01$ K (see Table 1). As discussed in Sect. 2, a galaxy solution with mass $M_h \simeq 10^6\ M_\odot$ exhibits quantum properties: it is near the quantum degenerate regime but is not in a zero temperature degenerate state, dwarf galaxies possessing a small but non-zero temperature.

Dwarf galaxies are macroscopic astrophysical quantum objects as white dwarf stars and neutron stars [32,33], but are different from them.

We find that all magnitudes in the diluted regime exhibit square-root of M_h **scaling** laws and are **universal** functions of r/r_h normalized to their values at the origin or at r_h. Conversely, the halo mass M_h scales as the square of the halo radius r_h as

$$M_h = 1.75572\ \Sigma_0\ r_h^2.$$

Moreover, the proportionality factor in this scaling relation is confirmed by the galaxy data (see Fig. 2).

We find that the universal theoretical density profile obtained from the Thomas–Fermi equation (1.1) in the diluted regime ($M_h \gtrsim 10^6\ M_\odot$) is accurately reproduced by the simple formula (see Fig. 5)

$$\frac{\rho(r)}{\rho(0)} = \frac{1}{\left[1 + \left(4^{\frac{1}{\alpha}} - 1\right)\left(\frac{r}{r_h}\right)^2\right]^\alpha}, \quad \alpha = 1.5913.$$

The fit is precise for $r < 2\ r_h$.

The theoretical rotation curves and density profiles obtained from the Thomas–Fermi equations remarkably agree with observations for $r \lesssim r_h$, for all galaxies in the diluted regime [40]. This indicates that WDM is thermalized in the internal regions $r \lesssim r_h$ of galaxies.

We find the WDM galaxy equation of state, that is, the functional relation between the pressure P and the density ρ in a parametric way as

$$\rho = \frac{m^{\frac{5}{2}}}{3\pi^2\hbar^3} (2\ T_0)^{\frac{3}{2}}\ I_2(\nu), \quad P = \frac{m^{\frac{3}{2}}}{15\pi^2\hbar^3} (2\ T_0)^{\frac{5}{2}}\ I_4(\nu). \tag{1.17}$$

These equations express parametrically, through the parameter ν, the pressure P as a function of the density ρ and therefore provide the equation of state. $I_2(\nu)$ and $I_4(\nu)$ are integrals (2nd and 4th momenta) of the distribution function. At thermal equilibrium they are given by Eq. (2.15). For the main galaxy physical magnitudes, the Fermi–Dirac distribution gives similar results than the out of equilibrium distribution functions [31]. We plot in Figs. 7 and 8 P as a function of ρ for different values of the effective temperature T_0.

Interestingly enough, we provide a simple formula representing the exact equation of state (1.17) obtained by solving the Thomas–Fermi equation (1.1)

$$P = \frac{m^{\frac{3}{2}}\,(2\,T_0)^{\frac{5}{2}}}{15\,\pi^2\,\hbar^3}\,\left(1+\frac{3}{2}\,e^{-\beta_1\,\tilde{\rho}}\right)\,\tilde{\rho}^{\,\frac{1}{3}(5-2\,e^{-\beta_2\,\tilde{\rho}})}, \tag{1.18}$$

where

$$\tilde{\rho} \equiv \frac{3\,\pi^2\,\hbar^3}{m^{\frac{5}{2}}\,(2\,T_0)^{\frac{3}{2}}}\,\rho = I_2(\nu), \tag{1.19}$$

and the best fit to the exact values of P as a function $\tilde{\rho}$ is obtained for the values of the parameters

$$\beta_1 = 0.047098, \quad \beta_2 = 0.064492. \tag{1.20}$$

The fitting formula Eq. (1.18) exactly fulfills the diluted and degenerate limiting behaviors:

$$P = \frac{T_0}{m}\,\rho \quad \text{WDM diluted galaxies},$$

$$P = \frac{\hbar^2}{5}\,\left(\frac{3\,\pi^2}{m^4}\right)^{\frac{2}{3}}\,\rho^{\frac{5}{3}} \quad \text{WDM degenerate quantum limit}.$$

We plot in Fig. 9 the exact equation of state obtained by solving the Thomas–Fermi equation and the empirical equation of state equation (1.18).

We find that the presence of universal profiles in galaxies reflect the perfect gas behavior of the WDM galaxy equation of state in the diluted regime which is identical to the self-gravitating Boltzman WDM gas.

These theoretical results contrasted to robust and independent sets of galaxy data remarkably reproduce the observations.

For the small galaxies, $10^6\ M_\odot \gtrsim M_h \geq M_{h,\min}$ corresponding to effective temperatures $T_0 \lesssim 0.017$ K, the equation of state is steeper, dependent on the galaxy mass and the profiles are not anymore universal. These non-universal properties in small galaxies account to the quantum physics of the self-gravitating WDM fermions in the compact regime with high density close to, but not at, the degenerate state.

It would be extremely interesting to dispose of observations which could check these quantum effects in dwarf galaxies.

In summary, the results of this paper show the power and cleanliness of the Thomas–Fermi theory and WDM to properly describe the galaxy structures and the galaxy physical states.

This paper is organized as follows. In Sect. 2 we present the Thomas–Fermi approach to galaxy structure, we express the main galaxy magnitudes in terms of the solution of the Thomas–Fermi equation and the value of the surface density Σ_0. We analyze the diluted classical galaxy magnitudes, derive their scaling laws and find the universal density and velocity profiles and their agreement with observations.

In Sect. 3 we derive the equation of state of galaxies and analyze their main regimes: classical regime which is the perfect inhomogeneous equation of state, identical to the WDM self-gravitating gas equation of state, and the quantum regime, which exhibits a steeper equation of state, non-universal, galaxy mass dependent and describes the quantum fermionic compact states (dwarf galaxies), close to the degenerate limit. Finally, the invariance and dependence on the WDM particle mass m in the classical and quantum regimes is discussed.

2 Galaxy structure in the WDM Thomas–Fermi approach

We consider DM dominated galaxies in their late stages of structure formation when they are relaxing to a stationary situation, at least not too far from the galaxy center.

This is a realistic situation since the free-fall (Jeans) time t_{ff} for galaxies is much shorter than the age of galaxies:

$$t_{ff} = \frac{1}{\sqrt{G\,\rho_0}} = 1.49\times 10^7\,\sqrt{\frac{M_\odot}{\rho_0\ \mathrm{pc}^3}}\ \text{year}.$$

The observed central densities of galaxies yield free-fall times in the range from 15 million years for ultracompact galaxies till 330 million years for large diluted spiral galaxies. These free-fall (or collapse) times are small compared with the age of galaxies running in billions of years.

Hence, we can consider the DM described by a time-independent and non-relativistic energy distribution function $f(E)$, where $E = p^2/(2m) - \mu$ is the single-particle energy, m is the mass of the DM particle and μ is the chemical potential [30,31] related to the gravitational potential $\phi(\mathbf{r})$ by

$$\mu(\mathbf{r}) = \mu_0 - m\,\phi(\mathbf{r}), \tag{2.1}$$

where μ_0 is a constant.

In the Thomas–Fermi approach, $\rho(\mathbf{r})$ is expressed as a function of $\mu(\mathbf{r})$ through the standard integral of the DM phase-space distribution function over the momentum

$$\rho(\mathbf{r}) = \frac{g\,m}{2\,\pi^2\,\hbar^3}\int_0^\infty \mathrm{d}p\ p^2\ f\left[\frac{p^2}{2m} - \mu(\mathbf{r})\right], \tag{2.2}$$

where g is the number of internal degrees of freedom of the DM particle, with $g = 1$ for Majorana fermions and $g = 2$ for Dirac fermions.

We will consider spherical symmetric configurations. Then the Poisson equation for $\phi(r)$ takes the self-consistent form

$$\frac{\mathrm{d}^2\mu}{\mathrm{d}r^2}+\frac{2}{r}\,\frac{\mathrm{d}\mu}{\mathrm{d}r}=-4\pi\,G\,m\,\rho(r)=-\frac{2\,g\,G\,m^2}{\pi\,\hbar^3}\times\int_0^\infty \mathrm{d}p\;p^2\;f\left[\frac{p^2}{2m}-\mu(r)\right], \tag{2.3}$$

where G is Newton's constant and $\rho(r)$ is the DM mass density.

Equation (2.3) provides an ordinary **non-linear** differential equation that determines **self-consistently** the chemical potential $\mu(r)$ and constitutes the Thomas–Fermi approach [30,31] (see also Refs. [34–36]). This is a semiclassical approach to galaxy structure in which the quantum nature of the DM particles is taken into account through the quantum statistical distribution function $f(E)$.

The DM pressure and the velocity dispersion can also be expressed as integrals over the DM phase-space distribution function as

$$P(r)=\frac{g}{6\pi^2\,m\,\hbar^3}\int_0^\infty \mathrm{d}p\;p^4\;f\left[\frac{p^2}{2m}-\mu(r)\right], \tag{2.4}$$

$$\langle v^2\rangle(r)=\frac{1}{m^2}\,\frac{\int_0^\infty \mathrm{d}p\;p^4\;f\left[\frac{p^2}{2m}-\mu(r)\right]}{\int_0^\infty \mathrm{d}p\;p^2\;f\left[\frac{p^2}{2m}-\mu(r)\right]}. \tag{2.5}$$

Equations (2.2), (2.4), and (2.5) imply the equation of state

$$P(r)=\frac{1}{3}\langle v^2\rangle(r)\;\rho(r)=\sigma^2(r)\;\rho(r). \tag{2.6}$$

It must be stressed that the Thomas–Fermi equation (2.3) determine $\sigma^2(r)$ in terms of $\rho(r)$ through Eq. (2.5). Therefore, the Thomas–Fermi equation **determines the equation of state** through Eq. (2.6). Contrary to the usual situation [41], we **do not assume** the equation of state, but we **derive** it from the Thomas–Fermi equation.

The fermionic DM mass density ρ is bounded at the origin due to the Pauli principle [30] which implies the bounded boundary condition at the origin

$$\frac{\mathrm{d}\mu}{\mathrm{d}r}(0)=0. \tag{2.7}$$

We see that $\mu(r)$ fully characterizes the DM halo structure in this Thomas–Fermi framework. The chemical potential is monotonically decreasing in r since Eq. (2.3) implies

$$\frac{\mathrm{d}\mu}{\mathrm{d}r}=-\frac{G\,m\,M(r)}{r^2},\quad M(r)=4\pi\int_0^r \mathrm{d}r'\,r'^2\,\rho(r'). \tag{2.8}$$

From Eqs. (2.4) and (2.5) we derive the hydrostatic equilibrium equation

$$\frac{\mathrm{d}P}{\mathrm{d}r}+\rho(r)\,\frac{\mathrm{d}\phi}{\mathrm{d}r}=0. \tag{2.9}$$

Eliminating $P(r)$ between Eqs. (2.6) and (2.9) and integrating on r gives

$$\frac{\rho(r)}{\rho(0)}=\frac{\sigma^2(0)}{\sigma^2(r)}\,\mathrm{e}^{-\int_0^r \frac{\mathrm{d}r'}{\sigma^2(r')}\,\frac{\mathrm{d}\phi}{\mathrm{d}r'}}. \tag{2.10}$$

Inserting this expression in the Poisson equation yields

$$\frac{\mathrm{d}^2\phi}{\mathrm{d}r^2}+\frac{2}{r}\,\frac{\mathrm{d}\phi}{\mathrm{d}r}=4\,\pi\;G\;\rho_0\,\frac{\sigma^2(0)}{\sigma^2(r)}\,\mathrm{e}^{-\int_0^r \frac{\mathrm{d}r'}{\sigma^2(r')}\,\frac{\mathrm{d}\phi}{\mathrm{d}r'}}. \tag{2.11}$$

This non-linear equation for non-constant $\sigma^2(r)$ generalizes the corresponding equation in the self-gravitating Boltzmann gas. For constant $\sigma^2(r)$ Eq. (2.10) reduces to the barotropic equation.

In this semiclassical framework the stationary energy distribution function $f(E)$ must be given. We consider the Fermi–Dirac distribution,

$$f(E)=\Psi_{\mathrm{FD}}(E/T_0)=\frac{1}{\mathrm{e}^{E/T_0}+1}, \tag{2.12}$$

where the characteristic one-particle energy scale T_0 in the DM halo plays the role of an effective temperature. The value of T_0 depends on the galaxy mass. In neutron stars, where the neutron mass is about six orders of magnitude larger than the WDM particle mass, the temperature can be approximated by zero. In galaxies, $T_0\sim m\;<v^2>$ turns to be non-zero but small in the range: $10^{-3}\ \mathrm{K}\lesssim T_0\lesssim 10\ \mathrm{K}$ for halo galaxy masses in the range 10^5–$10^{12}\ M_\odot$, which reproduce the observed velocity dispersions for $m\simeq 2$ keV. The smaller values of T_0 correspond to compact dwarfs and the larger values of T_0 are for large and diluted galaxies.

Notice that, for the relevant galaxy physical magnitudes, the Fermi–Dirac distribution gives similar results than the out of equilibrium distribution functions [31].

The choice of Ψ_{FD} is justified in the inner regions, where relaxation to thermal equilibrium is possible. Far from the origin, however, the Fermi–Dirac distribution as its classical counterpart, the isothermal sphere, produces a mass density tail $1/r^2$, which overestimates the observed tails of the galaxy mass densities. Indeed, the classical regime $\mu/T_0\to-\infty$ is attained for large distances r since Eq. (2.8) indicates that $\mu(r)$ is always monotonically decreasing with r.

More precisely, large positive values of the chemical potential at the origin correspond to the degenerate fermions limit which is the extreme quantum case and oppositely, large

negative values of the chemical potential at the origin gives the diluted case which is the classical regime. The quantum degenerate regime describes dwarf and compact galaxies while the classical and diluted regime describes large and diluted galaxies. In the classical regime, the Thomas–Fermi equations (2.3)–(2.7) become the equations for a self-gravitating Boltzmann gas.

It is useful to introduce dimensionless variables $\xi,\ \nu(\xi)$

$$r = l_0\,\xi, \quad \mu(r) = T_0\,\nu(\xi), \quad f(E) = \Psi(E/T_0), \tag{2.13}$$

where l_0 is the characteristic length that emerges from the dynamical equation (2.3):

$$\begin{aligned} l_0 &\equiv \frac{\hbar}{\sqrt{8\,G}}\,\left(\frac{2}{g}\right)^{\frac{1}{3}}\,\left[\frac{9\,\pi\ I_2(\nu_0)}{m^8\,\rho_0}\right]^{\frac{1}{6}} \\ &= R_0\left(\frac{2\,\mathrm{keV}}{m}\right)^{\frac{4}{3}}\,\left(\frac{2}{g}\right)^{\frac{1}{3}}\,\left[\frac{I_2(\nu_0)}{\rho_0}\,\frac{M_\odot}{\mathrm{pc}^3}\right]^{\frac{1}{6}}, \\ R_0 &= 7.425\ \mathrm{pc}, \end{aligned} \tag{2.14}$$

and

$$\begin{aligned} I_n(\nu) &\equiv (n+1)\,\int_0^\infty y^n\,\mathrm{d}y\ \Psi_{FD}(y^2-\nu), \\ n &= 1, 2, \ldots\ , \quad \nu_0 \equiv \nu(0), \quad \rho_0 = \rho(0), \end{aligned} \tag{2.15}$$

where we use the integration variable $y \equiv p/\sqrt{2\,m\,T_0}$. For definiteness, we will take $g = 2$, Dirac fermions in the sequel. One can easily translate from Dirac to Majorana fermions changing the WDM fermion mass as

$$m \Rightarrow \frac{m}{2^{\frac{1}{4}}} = 0.8409\ m.$$

Then, in dimensionless variables, the self-consistent Thomas–Fermi equation (2.3) for the chemical potential $\nu(\xi)$ takes the form

$$\frac{\mathrm{d}^2\nu}{\mathrm{d}\xi^2} + \frac{2}{\xi}\,\frac{\mathrm{d}\nu}{\mathrm{d}\xi} = -I_2(\nu), \quad \nu'(0) = 0. \tag{2.16}$$

We find the main physical galaxy magnitudes, such as the mass density $\rho(r)$, the velocity dispersion $\sigma^2(r) = v^2(r)/3$ and the pressure $P(r)$, which are all r-dependent:

$$\begin{aligned} \rho(r) &= \frac{m^{\frac{5}{2}}}{3\,\pi^2\,\hbar^3}\ (2\ T_0)^{\frac{3}{2}}\ I_2(\nu(\xi)) = \rho_0\ \frac{I_2(\nu(\xi))}{I_2(\nu_0)}, \\ \rho_0 &= \frac{m^{\frac{5}{2}}}{3\,\pi^2\,\hbar^3}\ (2\ T_0)^{\frac{3}{2}}\ I_2(\nu_0), \end{aligned} \tag{2.17}$$

$$\begin{aligned} P(r) &= \frac{m^{\frac{3}{2}}}{15\,\pi^2\,\hbar^3}\ (2\ T_0)^{\frac{5}{2}}\ I_4(\nu(\xi)) = \frac{1}{5}\ \left(9\,\pi^4\right)^{\frac{1}{3}} \\ &\times \left(\frac{\hbar^6}{m^8}\right)^{\frac{1}{3}}\ \left[\frac{\rho_0}{I_2(\nu_0)}\right]^{5/3}\ I_4(\nu(\xi)), \end{aligned} \tag{2.18}$$

$$\sigma^2(r) = \frac{P(r)}{\rho(r)} = \frac{2\ T_0}{5\ m}\ \frac{I_4(\nu(\xi))}{I_2(\nu(\xi))}. \tag{2.19}$$

As a consequence, from Eqs. (2.8), (2.13), (2.14), (2.17), and (2.19) the total mass $M(r)$ enclosed in a sphere of radius r and the phase space density $Q(r)$ turn out to be

$$\begin{aligned} M(r) &= 4\,\pi\ \frac{\rho_0\ l_0^3}{I_2(\nu_0)}\ \int_0^\xi \mathrm{d}x\ x^2\ I_2(\nu(x)) \\ &= 4\,\pi\ \frac{\rho_0\ l_0^3}{I_2(\nu_0)}\ \xi^2\ |\nu'(\xi)| \\ &= M_0\ \xi^2\ |\nu'(\xi)|\ \left(\frac{\mathrm{keV}}{m}\right)^4\ \sqrt{\frac{\rho_0}{I_2(\nu_0)}\,\frac{\mathrm{pc}^3}{M_\odot}}, \end{aligned} \tag{2.20}$$

$$M_0 = 4\,\pi\ M_\odot\ \left(\frac{R_0}{\mathrm{pc}}\right)^3 = 0.8230\times 10^5\ M_\odot, \tag{2.21}$$

$$Q(r) \equiv \frac{\rho(r)}{\sigma^3(r)} = 3\,\sqrt{3}\ \frac{\rho(r)}{\langle v^2\rangle^{\frac{3}{2}}(r)} = \frac{\sqrt{125}}{3\,\pi^2}\ \frac{m^4}{\hbar^3}\ \frac{I_2^{\frac{5}{2}}(\nu(\xi))}{I_4^{\frac{3}{2}}(\nu(\xi))}. \tag{2.22}$$

In these expressions, we have systematically eliminated the energy scale T_0 in terms of the central density ρ_0 through Eq. (2.17). Notice that $Q(r)$ turns to be independent of T_0 and therefore of ρ_0.

We define the core size r_h of the halo by analogy with the Burkert density profile as

$$\frac{\rho(r_h)}{\rho_0} = \frac{1}{4}, \quad r_h = l_0\,\xi_h. \tag{2.23}$$

It must be noticed that the surface density

$$\Sigma_0 \equiv r_h\ \rho_0 \tag{2.24}$$

is found to be nearly **constant** and independent of the luminosity in different galactic systems (spirals, dwarf irregular and spheroidals, elliptics) spanning over 14 magnitudes in luminosity and over different Hubble types. More precisely, all galaxies seem to have the same value for Σ_0, namely $\Sigma_0 \simeq 120\ M_\odot/\mathrm{pc}^2$ up to 10–20% [38,39,42]. It is remarkable that at the same time other important structural quantities as $r_h,\ \rho_0$, the baryon-fraction and the galaxy mass vary orders of magnitude from one galaxy to another.

The constancy of Σ_0 seems unlikely to be a mere coincidence and probably reflects a physical scaling relation between the mass and halo size of galaxies. It must be stressed that Σ_0 is the only dimensionful quantity which is constant among the different galaxies.

It is then useful to take here the dimensionful quantity Σ_0 as physical scale to express the galaxy magnitudes in the Thomas–Fermi approach. That is, we replace the central density ρ_0 in the above galaxy magnitudes Eqs. (2.14)–(2.21) in terms of Σ_0 Eq. (2.24) with the following results:

$$l_0 = \left(\frac{9\,\pi}{2^9}\right)^{\frac{1}{5}} \left(\frac{\hbar^6}{G^3\,m^8}\right)^{\frac{1}{5}} \left[\frac{\xi_h\; I_2(\nu_0)}{\Sigma_0}\right]^{\frac{1}{5}}$$
$$= 4.2557\;\left[\xi_h\; I_2(\nu_0)\right]^{\frac{1}{5}} \left(\frac{2\,\mathrm{keV}}{m}\right)^{\frac{8}{5}} \left(\frac{120\;M_\odot}{\Sigma_0\;\mathrm{pc}^2}\right)^{\frac{1}{5}}\;\mathrm{pc}, \tag{2.25}$$

$$T_0 = \left(18\,\pi^6\,\frac{\hbar^6\;G^2}{m^3}\right)^{\frac{1}{5}} \left[\frac{\Sigma_0}{\xi_h\; I_2(\nu_0)}\right]^{\frac{4}{5}}$$
$$= \frac{7.12757\;10^{-3}}{\left[\xi_h\; I_2(\nu_0)\right]^{\frac{4}{5}}} \left(\frac{2\,\mathrm{keV}}{m}\right)^{\frac{3}{5}} \left(\frac{\Sigma_0\;\mathrm{pc}^2}{120\;M_\odot}\right)^{\frac{4}{5}}\;\mathrm{K} \tag{2.26}$$

and

$$r = 4.2557\;\xi\;\left[\xi_h\; I_2(\nu_0)\right]^{\frac{1}{5}} \left(\frac{2\,\mathrm{keV}}{m}\right)^{\frac{8}{5}}$$
$$\times \left(\frac{120\;M_\odot}{\Sigma_0\;\mathrm{pc}^2}\right)^{\frac{1}{5}}\;\mathrm{pc}\;, \tag{2.27}$$

$$\rho(r) = \left(\frac{2^9\;G^3\;m^8}{9\;\pi\;\hbar^6}\right)^{\frac{1}{5}} \left[\frac{\Sigma_0}{\xi_h\; I_2(\nu_0)}\right]^{\frac{6}{5}} I_2(\nu(\xi))$$
$$= 18.1967\;\frac{I_2(\nu(\xi))}{\left[\xi_h\; I_2(\nu_0)\right]^{\frac{6}{5}}} \left(\frac{m}{2\,\mathrm{keV}}\right)^{\frac{8}{5}}$$
$$\times \left(\frac{\Sigma_0\;\mathrm{pc}^2}{120\;M_\odot}\right)^{\frac{6}{5}} \frac{M_\odot}{\mathrm{pc}^3}, \tag{2.28}$$

$$M(r) = 4\,\pi\;\left(\frac{9\;\pi\;\hbar^6}{2^9\;G^3\;m^8}\right)^{\frac{2}{5}} \left[\frac{\Sigma_0}{\xi_h\; I_2(\nu_0)}\right]^{\frac{3}{5}} \xi^2\;|\nu'(\xi)|$$
$$= \frac{27312\;\xi^2}{\left[\xi_h\; I_2(\nu_0)\right]^{\frac{3}{5}}}\;|\nu'(\xi)|\;\left(\frac{2\,\mathrm{keV}}{m}\right)^{\frac{16}{5}}$$
$$\times \left(\frac{\Sigma_0\;\mathrm{pc}^2}{120\;M_\odot}\right)^{\frac{3}{5}} M_\odot\;, \tag{2.29}$$

$$\sigma^2(r) = \frac{11.0402}{\left[\xi_h\; I_2(\nu_0)\right]^{\frac{4}{5}}}\;\frac{I_4(\nu(\xi))}{I_2(\nu(\xi))}\;\left(\frac{2\,\mathrm{keV}}{m}\right)^{\frac{8}{5}}$$
$$\times \left(\frac{\Sigma_0\;\mathrm{pc}^2}{120\;M_\odot}\right)^{\frac{4}{5}} \left(\frac{\mathrm{km}}{\mathrm{s}}\right)^2, \tag{2.30}$$

$$P(r) = \frac{8\,\pi}{5}\;G\;\left[\frac{\Sigma_0}{\xi_h\; I_2(\nu_0)}\right]^2 I_4(\nu(\xi))$$
$$= \frac{200.895}{\left[\xi_h\; I_2(\nu_0)\right]^2}\;I_4(\nu(\xi))\;\left(\frac{\Sigma_0\;\mathrm{pc}^2}{120\;M_\odot}\right)^2$$
$$\times \frac{M_\odot}{\mathrm{pc}^3}\;\left(\frac{\mathrm{km}}{\mathrm{s}}\right)^2. \tag{2.31}$$

For a fixed value of the surface density Σ_0, the solutions of the Thomas–Fermi equation (2.16) are parametrized by a single parameter: the dimensionless chemical potential at the origin ν_0. The value of ν_0 at fixed Σ_0 can be determined by the value of the halo galaxy mass $M(r_h)$ obtained from Eq. (2.29) at $r = r_h$. We have

$$M_h \equiv M(r_h) = \frac{27312\;\xi_h^{\frac{7}{5}}}{\left[I_2(\nu_0)\right]^{\frac{3}{5}}}\;|\nu'(\xi_h)|\;\left(\frac{2\,\mathrm{keV}}{m}\right)^{\frac{16}{5}}$$
$$\times \left(\frac{\Sigma_0\;\mathrm{pc}^2}{120\;M_\odot}\right)^{\frac{3}{5}} M_\odot. \tag{2.32}$$

Also, at fixed surface density Σ_0, the effective temperature T_0 is only a function of ν_0.

It is useful to introduce the rescaled dimensionless variables

$$\hat{r}_h \equiv r_h\;\left(\frac{m}{2\,\mathrm{keV}}\right)^{\frac{8}{5}} \left(\frac{\Sigma_0\;\mathrm{pc}^2}{120\;M_\odot}\right)^{\frac{1}{5}},$$
$$\hat{M}_h \equiv M_h\;\left(\frac{m}{2\,\mathrm{keV}}\right)^{\frac{16}{5}} \left(\frac{120\;M_\odot}{\Sigma_0\;\mathrm{pc}^2}\right)^{\frac{3}{5}}$$
$$\hat{T}_0 \equiv T_0\;\frac{2\,\mathrm{keV}}{m}\;\left(\frac{120\;M_\odot}{\Sigma_0\;\mathrm{pc}^2}\right)^{\frac{4}{5}}$$
$$\hat{\nu}_0 \equiv \nu_0 + 4\;\ln\left(\frac{m}{2\,\mathrm{keV}}\right),$$
$$\hat{\sigma}^2(r) \equiv \sigma^2(r)\;\left(\frac{m}{2\,\mathrm{keV}}\right)^{\frac{8}{5}} \left(\frac{120\;M_\odot}{\Sigma_0\;\mathrm{pc}^2}\right)^{\frac{4}{5}}. \tag{2.33}$$

We display in Table 1 the corresponding values of the halo mass $\hat{M}_h$, the effective temperature $\hat{T}_0$ and the chemical potential at the origin ν_0 in the whole galaxy mass range, from large diluted galaxies till small ultracompact galaxies.

The circular velocity $v_c(r)$ is defined through the virial theorem as

$$v_c(r) \equiv \sqrt{\frac{G\;M(r)}{r}}, \tag{2.34}$$

and it is directly related by Eq. (2.8) to the derivative of the chemical potential as

$$v_c(r) = \sqrt{-\frac{r}{m}\;\frac{\mathrm{d}\mu}{\mathrm{d}r}} = \sqrt{-\frac{T_0}{m}\;\frac{\mathrm{d}\nu}{d\,\ln\xi}}.$$

Expressing T_0 in terms of the surface density Σ_0 using Eq. (2.26) we have for the circular velocity the explicit expression

$$v_c(r) = 5.2537\;\frac{\sqrt{-\xi\;\nu'(\xi)}}{\left[\xi_h\; I_2(\nu_0)\right]^{\frac{2}{5}}}\;\left(\frac{2\,\mathrm{keV}}{m}\right)^{\frac{4}{5}} \left(\frac{\Sigma_0\;\mathrm{pc}^2}{120\;M_\odot}\right)^{\frac{2}{5}}\;\frac{\mathrm{km}}{\mathrm{s}} \tag{2.35}$$

and the rescaled circular velocity

$$\hat{v}_c^2(r) \equiv v_c^2(r)\;\left(\frac{m}{2\,\mathrm{keV}}\right)^{\frac{8}{5}} \left(\frac{120\;M_\odot}{\Sigma_0\;\mathrm{pc}^2}\right)^{\frac{4}{5}}.$$

Two important combinations of galaxy magnitudes are $r\;\rho(r')$ and $M(r)/[4\,\pi\;r^2]$. From Eqs. (2.13), (2.20), (2.25),

and (2.28) we obtain

$$r\ \rho(r') = \Sigma_0\ \frac{\xi\ I_2(\nu(\xi'))}{\xi_h\ I_2(\nu_0)},\quad \frac{M(r)}{4\pi\ r^2} = \Sigma_0\ \frac{|\nu'(\xi)|}{\xi_h\ I_2(\nu_0)}. \tag{2.36}$$

In particular, it follows that $r_h\ \rho(0) = \Sigma_0$ reproducing the surface density as it must. At a generic point r Eq. (2.36) provide expressions for a space-dependent surface density. They are both proportional to Σ_0 and differ from each other by factors of order one. Notice that $\hbar$, G and m canceled out in these space-dependent surface densities Eq. (2.36).

2.1 Galaxy properties in the diluted Boltzmann regime

In the diluted Boltzmann regime, $\nu_0 \lesssim -5$, the analytic expressions for the main galaxies magnitudes are given by

$$M_h = 1.75572\ \Sigma_0\ r_h^2,\quad r_h = 68.894\ \sqrt{\frac{M_h}{10^6\ M_\odot}\ \frac{120\ M_\odot}{\Sigma_0\ \mathrm{pc}^2}}\ \ \mathrm{pc}, \tag{2.37}$$

$$T_0 = 8.7615\ 10^{-3}\ \sqrt{\frac{M_h}{10^6\ M_\odot}}\ \frac{m}{2\,\mathrm{keV}}\ \sqrt{\frac{\Sigma_0\ \mathrm{pc}^2}{120\ M_\odot}}\ \mathrm{K}, \tag{2.38}$$

$$\rho(r) = 5.19505\ \left(\frac{M_h}{10^4\ M_\odot}\ \frac{\Sigma_0\ \mathrm{pc}^2}{120\ M_\odot}\right)^{\frac{3}{4}}\ \left(\frac{m}{2\,\mathrm{keV}}\right)^4\ e^{\nu(\xi)}\ \ \frac{M_\odot}{\mathrm{pc}^3}\ , \tag{2.39}$$

$$\sigma^2(r) = 33.927\ \sqrt{\frac{M_h}{10^6\ M_\odot}\ \frac{\Sigma_0\ \mathrm{pc}^2}{120\ M_\odot}}\ \left(\frac{\mathrm{km}}{\mathrm{s}}\right)^2, \tag{2.40}$$

$$v_c^2(r) = 33.9297\ \sqrt{\frac{M_h}{10^6\ M_\odot}\ \frac{\Sigma_0\ \mathrm{pc}^2}{120\ M_\odot}}\ \left|\frac{\mathrm{d}\nu(\xi)}{d\ln\xi}\right|\ \left(\frac{\mathrm{km}}{\mathrm{s}}\right)^2,$$

$$v_c^2(r_h) = 62.4292\ \sqrt{\frac{M_h}{10^6\ M_\odot}\ \frac{\Sigma_0\ \mathrm{pc}^2}{120\ M_\odot}}\ \left(\frac{\mathrm{km}}{\mathrm{s}}\right)^2 \tag{2.41}$$

$$M(r) = 7.88895\ \left|\frac{\mathrm{d}\nu(\xi)}{d\ln\xi}\right|\ \frac{r}{\mathrm{pc}}\ \sqrt{\frac{M_h}{10^6\ M_\odot}\ \frac{\Sigma_0\ \mathrm{pc}^2}{120\ M_\odot}}. \tag{2.42}$$

In addition, M_h and T_0 scale as functions of the fugacity at the center $z_0 = e^{\nu_0}$:

$$M_h \equiv M(r_h) = \frac{67014.6}{z_0^{\frac{4}{5}}}\ \left(\frac{2\,\mathrm{keV}}{m}\right)^{\frac{16}{5}}\ \left(\frac{\Sigma_0\ \mathrm{pc}^2}{120\ M_\odot}\right)^{\frac{3}{5}}\ M_\odot, \tag{2.43}$$

$$T_0 = \frac{2.2681\ 10^{-3}}{z_0^{\frac{2}{5}}}\ \left(\frac{2\,\mathrm{keV}}{m}\right)^{\frac{3}{5}}\ \left(\frac{\Sigma_0\ \mathrm{pc}^2}{120\ M_\odot}\right)^{\frac{4}{5}}\ \mathrm{K}. \tag{2.44}$$

Therefore, **all** these galaxy magnitudes **scale** as functions of each other.

For the equation of state and the phase space density we find the expressions

$$P(r) = 5.57359\ 10^3\ \left(\frac{M_h}{10^6\ M_\odot}\ \frac{\Sigma_0\ \mathrm{pc}^2}{120\ M_\odot}\right)^{\frac{5}{4}} \times \left(\frac{m}{2\,\mathrm{keV}}\right)^4\ \mathrm{e}^{\nu(\xi)}\ \ \frac{M_\odot}{\mathrm{pc}}^3\ \left(\frac{\mathrm{km}}{\mathrm{s}}\right)^2\ , \tag{2.45}$$

$$P_0 \equiv P(0) = 59.097\ \left(\frac{\Sigma_0\ \mathrm{pc}^2}{120\ M_\odot}\right)^2\ \frac{M_\odot}{\mathrm{pc}^3}\ \left(\frac{\mathrm{km}}{\mathrm{s}}\right)^2, \tag{2.46}$$

$$Q(r) = 2.031796\ \left(\frac{m}{2\,\mathrm{keV}}\right)^4\ e^{\nu(\xi)}\ \mathrm{keV}^4,$$

$$Q(0) = 1.2319\ \left(\frac{10^5\ M_\odot}{M_h}\right)^{\frac{5}{4}}\ \left(\frac{\Sigma_0\ \mathrm{pc}^2}{120\ M_\odot}\right)^{\frac{3}{4}}\ \mathrm{keV}^4\ . \tag{2.47}$$

These equations are accurate for $M_h \gtrsim 10^6\ M_\odot$. We see that they exhibit a **scaling** behavior for r_h, T_0, $Q(0)$, $\sigma^2(0)$ and $v_c^2(r_h)$ as functions of M_h.

We see from Eqs. (2.37) and (2.40) that T_0 and $m\ \sigma^2(0)$ only differ by purely numerical factors reflecting the equipartition of kinetic energy. More precisely, it follows from Eqs. (2.37) and (2.40) that

$$\frac{m}{2}\ \langle v^2(0)\rangle = \frac{3}{2}\ m\ \sigma^2(0) = \frac{3}{2}\ T_0, \tag{2.48}$$

which shows that in the diluted regime the self-gravitating WDM gas behaves as an **inhomogeneous perfect gas** as we will discuss in the next section.

We plot in Figs. 1 and 2, the dimensionless effective temperature $\hat{T}_0$, the chemical potential at the origin $\hat{\nu}_0$ and the normalized halo radius $\hat{r}_h$ as functions of the halo mass $\hat{M}_h$ as defined by Eq. (2.33). We also depict in Fig. 2 the galaxy observations from different sets of data from Refs. [20,21,43–50]. All data are well reproduced by our theoretical Thomas–Fermi results. The errors of the data can be estimated to be about 10–20%.

The characteristic temperature $\hat{T}_0$ monotonically grows with the halo mass $\hat{M}_h$ of the galaxy as shown by Fig. 1 and Eq. (2.43) following with good precision the square-root of $\hat{M}_h$ equation (2.37).

We see that the whole set of scaling behaviors of the diluted regime Eqs. (2.37)–(2.43) are **very accurate** except near the degenerate regime for halo masses $\hat{M}_h < 3 \times 10^5\ M_\odot$. The deviation from the diluted scaling regime for $\hat{M}_h < 3 \times 10^5\ M_\odot$ accounts for the quantum fermionic effects in the dwarf compact galaxies obtained in our Thomas–Fermi approach (Figs. 1, 2, 3).

It must be stressed that the scaling relations Eqs. (2.37)–(2.47) are a consequence solely of the self-gravitating interac-

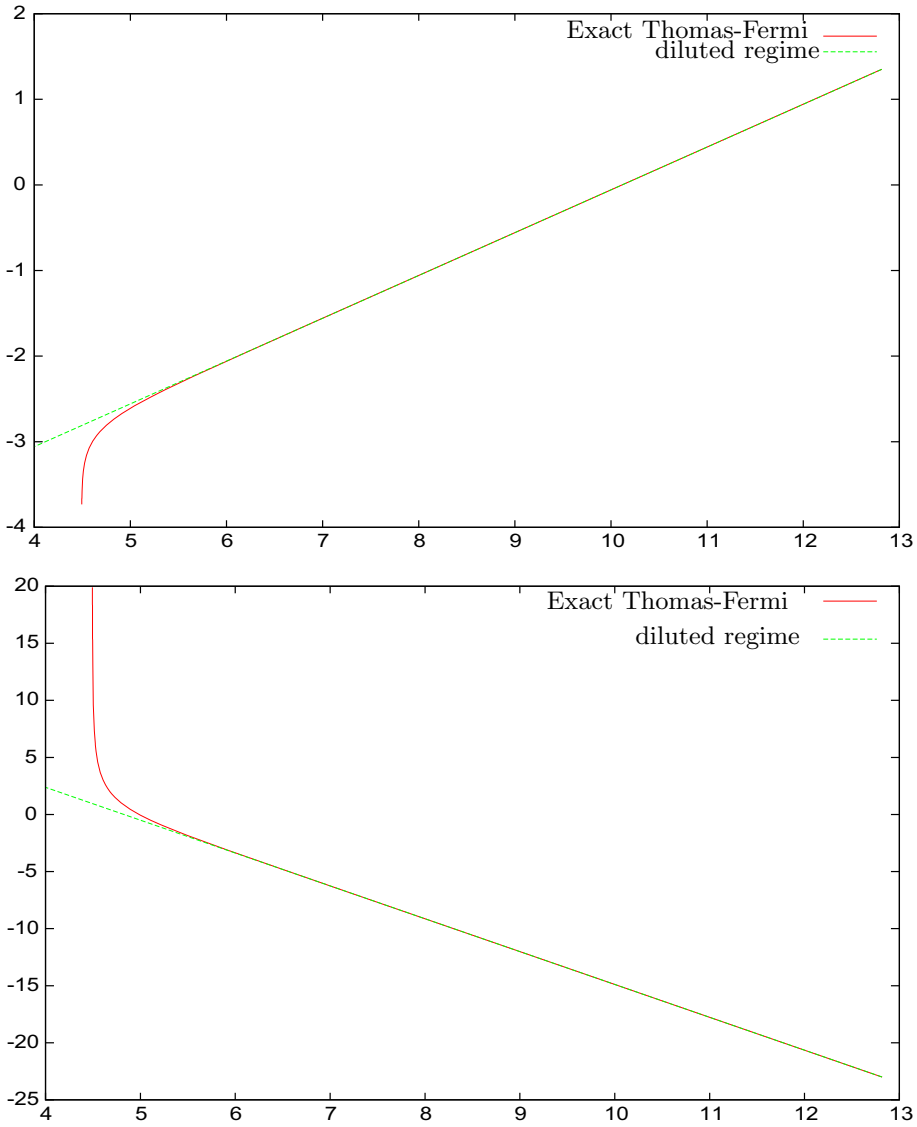

Fig. 1 *Upper panel* the common logarithm (base 10) of the effective temperature $\hat{T}_0$ (*vertical axis*) versus the common logarithm of the halo mass $\hat{M}_h$. We see that $\hat{T}_0$ grows with $\hat{M}_h$ following with precision the square-root of $\hat{M}_h$ law as in the diluted regime Eq. (2.37) of the Thomas–Fermi equations, except for $\hat{M}_h < 3 \times 10^5\ M_\odot,\ \nu_0 > -1.8,\ \hat{T}_0 < 0.005$ K, which is near the quantum degenerate regime and corresponds to compact dwarf galaxies. The deviation from the scaling diluted regime is due to the quantum fermionic effects which become important for dwarf compact galaxies. *Lower panel* the dimensionless chemical potential at the origin $\hat{\nu}_0$ versus the common (base 10) logarithm of $\hat{M}_h$. We see that ν_0 follows with precision the $(5/4)\log \hat{M}_h$ law as in the diluted regime equation (2.37) of the Thomas–Fermi equations except near the degenerate regime for $\hat{M}_h < 3 \times 10^5\ M_\odot,\ \nu_0 > -1.8,\ \hat{T}_0 < 0.005$ K corresponding to compact dwarf galaxies

tion of the fermionic WDM. Galaxy data verify the exponent and the amplitude factor in these scaling as shown in Fig. 2 for the square-root scaling relation Eq. (2.37).

It is highly remarkable that our theoretical results **reproduce** the observed DM halo properties with **good precision**.

The opposite limit, $\nu_0 \gtrsim 1$, is the quantum regime corresponding to compact WDM fermions. In particular, in the degenerate limit $\nu_0 \to \infty$, the galaxy mass and halo radius take their **minimum** values

$$r_h^{\min} = 11.3794 \left(\frac{2\,\text{keV}}{m}\right)^{\frac{8}{5}} \left(\frac{120\ M_\odot}{\Sigma_0\ \text{pc}^2}\right)^{\frac{1}{5}}\ \text{pc},$$
$$M_h^{\min} = 30{,}998.7 \left(\frac{2\,\text{keV}}{m}\right)^{\frac{16}{5}} \left(\frac{\Sigma_0\ \text{pc}^2}{120\ M_\odot}\right)^{\frac{3}{5}} M_\odot, \quad (2.49)$$

while the phase-space density $Q(r)$ takes its **maximum** value

$$Q_h^{\max} = 16\,\frac{\sqrt{125}}{3\,\pi^2} \left(\frac{m}{2\,\text{keV}}\right)^4\ \text{keV}^4$$
$$= 6.04163 \left(\frac{m}{2\,\text{keV}}\right)^4\ \text{keV}^4. \quad (2.50)$$

From the minimum value of the galaxy mass $M_h^{\min}$ we derive a lower bound for the WDM particle mass m

$$m \geq m_{\min} \equiv 1.387\ \text{keV} \left(\frac{10^5\ M_\odot}{M_h}\right)^{\frac{5}{16}} \left(\frac{\Sigma_0\ \text{pc}^2}{120\ M_\odot}\right)^{\frac{3}{16}}. \quad (2.51)$$

From the minimal known halo mass $M_h = 3.9 \times 10^4\ M_\odot$ for Willman I (see Table 1 in [31]) we obtain the lower bound

$m \geq 1.86$ keV for Dirac fermions,

$m \geq 2.21$ keV for Majorana fermions.

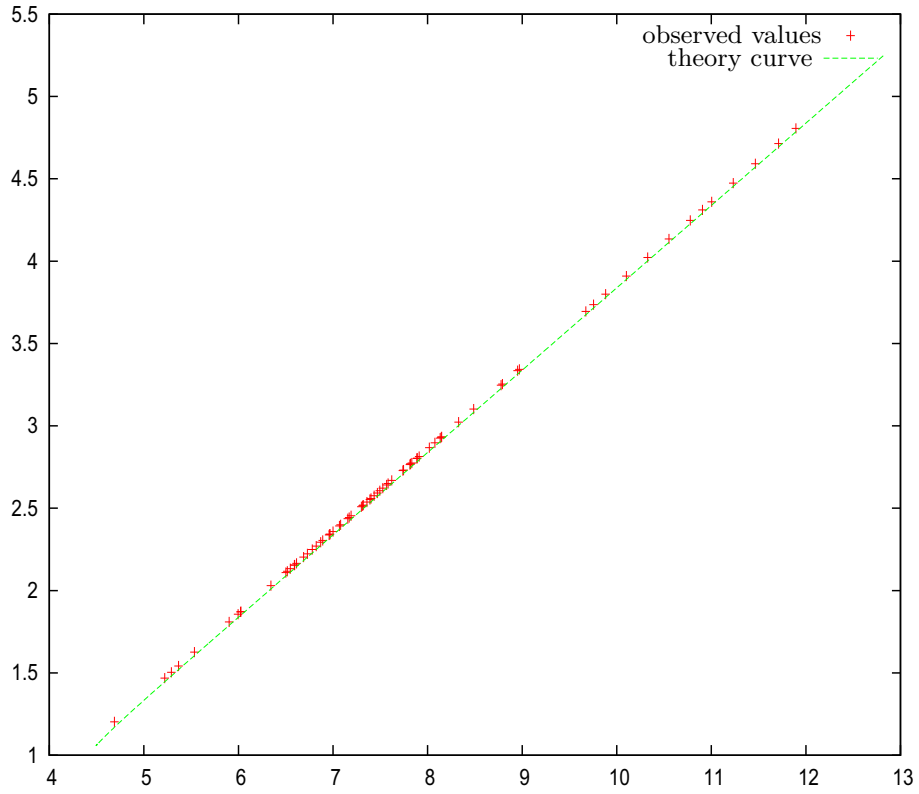

Fig. 2 The common logarithm (base 10) of the halo radius $\hat{r}_h = r_h \left(\frac{\Sigma_0\ \mathrm{pc}^2}{120\ M_\odot}\right)^{\frac{1}{5}}$ (*vertical axis*) vs. the common logarithm of the halo mass $\hat{M}_h = M_h \left(\frac{120\ M_\odot}{\Sigma_0\ \mathrm{pc}^2}\right)^{\frac{3}{5}}$. We see that r_h follows with precision the square-root of M_h law as in the diluted regime equation (2.37) of the Thomas–Fermi equations. In addition, the galaxy data confirm the proportionality factor in this scaling relation. The observational galaxy data for M_h and r_h are taken from Table 1 in [31] based on Refs. [20,21,43–50]. The data are very well reproduced by the theoretical Thomas–Fermi curve. The errors of the data can be estimated to be about 10–20%

Table 1 Corresponding values of the halo mass $\hat{M}_h$, the effective temperature $\hat{T}_0$ and the chemical potential at the origin ν_0 for WDM galaxies covering the whole range from large diluted galaxies till small ultracompact galaxies

$\hat{M}_h$	$\hat{T}_0$	$\nu_0 = \frac{\mu(0)}{T_0}$
$6.56 \times 10^{12}\ M_\odot$	22.4 K	−23
$6.45 \times 10^{11}\ M_\odot$	7.04 K	−20.1
$6.34 \times 10^{10}\ M_\odot$	2.21 K	−17.2
$4.9 \times 10^{9}\ M_\odot$	0.613 K	−14
$2.16 \times 10^{8}\ M_\odot$	0.129 K	−10.1
$1.55 \times 10^{7}\ M_\odot$	0.0344 K	−6.8
$3.67 \times 10^{6}\ M_\odot$	0.0168 K	−5
$1.66 \times 10^{6}\ M_\odot$	0.0112 K	−4
$1.21 \times 10^{5}\ M_\odot$	0.00278 K	−0.4
$9.73 \times 10^{4}\ M_\odot$	0.00241 K	0
$6.31 \times 10^{4}\ M_\odot$	0.00173 K	1
$4.06 \times 10^{4}\ M_\odot$	0.00101 K	3
$3.48 \times 10^{4}\ M_\odot$	6.82×10^{-4} K	5
$3.19 \times 10^{4}\ M_\odot$	3.63×10^{-4} K	10
$3.12 \times 10^{4}\ M_\odot$	1.84×10^{-4} K	20
$\hat{M}_h^{\min} = 3.10 \times 10^{4}\ M_\odot$	0	$+\infty$

3 Density and velocity dispersion: universal and non-universal profiles

It is illuminating to normalize the density profiles as $\rho(r)/\rho(0)$ and plot them as functions of r/r_h. We find that these normalized profiles are **universal** functions of $x \equiv r/r_h$ in the diluted regime as shown in Fig. 4. This universality is valid for **all** galaxy masses $\hat{M}_h > 10^5\ M_\odot$.

No analytic form is available for the profile $\rho(r)$ obtained from the resolution of the Thomas–Fermi equations (2.16). The universal profile $F(x) = \rho(r)/\rho(0)$ can be fitted with precision by the simple formula

$$F_\alpha(x) = \frac{1}{\left[1 + \left(4^{\frac{1}{\alpha}} - 1\right)\ x^2\right]^\alpha}, \quad x = \frac{r}{r_h}, \quad \alpha = 1.5913. \tag{3.1}$$

The value $\alpha = 1.5913$ provides the best fit. We plot in Fig. 5 $\rho(r)/\rho(0)$ from the Thomas–Fermi equations (2.16) and the precise fitting formula $F_{\alpha=1.5913}(x)$. The fit is particularly precise for $r < 2\ r_h$.

Our theoretical density profiles and rotation curves obtained from the Thomas–Fermi equations remarkably agree with

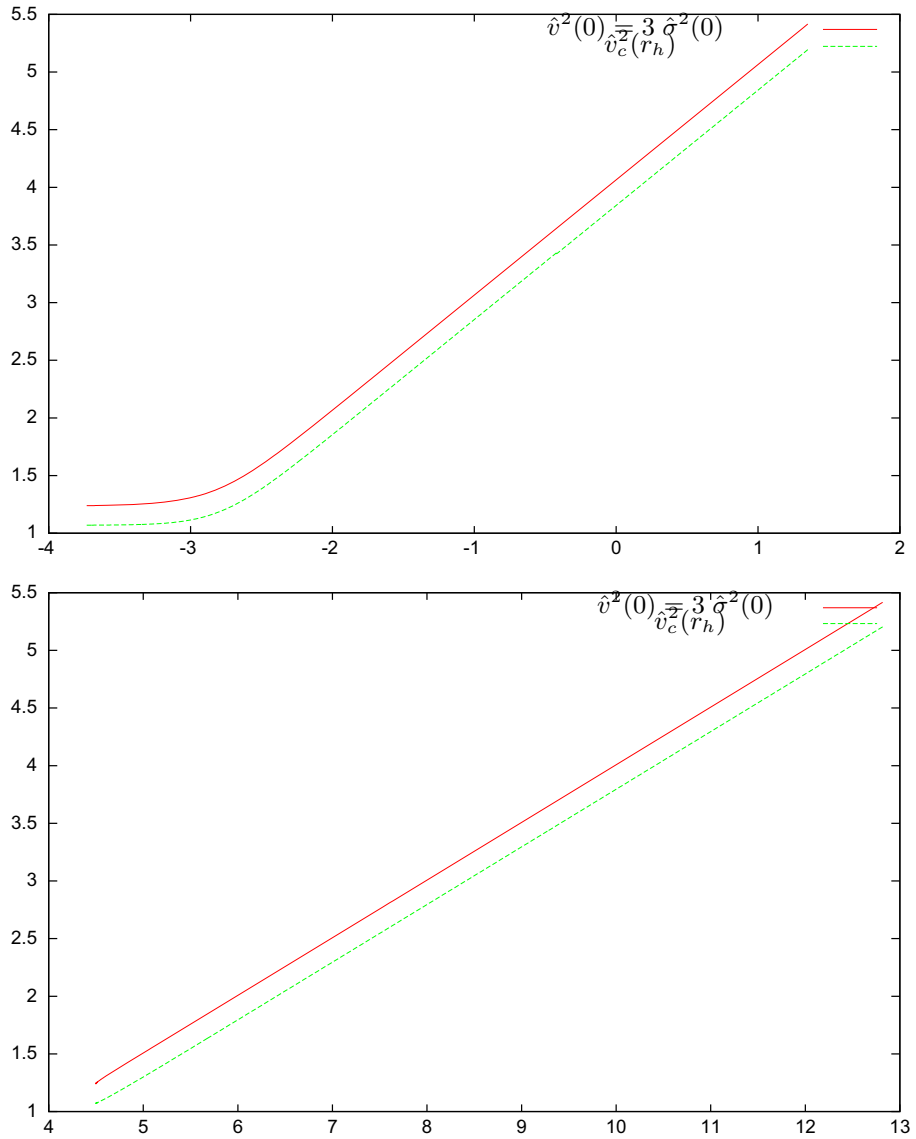

Fig. 3 *Upper panel* the common logarithm (base 10) of the velocity dispersion at the origin $\hat{v}^2(0) = 3\,\hat{\sigma}^2(0)$ and the common logarithm of the circular velocity at the halo radius $\hat{v}_c^2(r_h)$ versus $\log_{10}\hat{T}_0$. *Lower panel* the common logarithm (base 10) of the velocity dispersion at the origin $\hat{v}^2(0) = 3\,\hat{\sigma}^2(0)$ and the common logarithm of the circular velocity at the halo radius $\hat{v}_c^2(r_h)$ versus $\log_{10}\hat{M}_h$. Notice the unit slope in the *upper panel curves* as functions of $\hat{T}_0$ according to Eq. (3.3) in the diluted regime, and the one-half slope in the *lower panel curves* as functions of $\hat{M}_h$ following Eqs. (2.40) and (2.41) in the diluted regime. The deviation from the diluted scaling regime near the degenerate regime is manifest as a function of $\hat{T}_0$ (*upper panel*) while it is imperceptible as a function of $\hat{M}_h$ (*lower panel*)

observations for $r \lesssim r_h$, for all galaxies in the diluted regime [40]. This indicates that WDM is thermalized in the internal regions $r \lesssim r_h$ of galaxies.

The theoretical profile $\rho(r)/\rho(0)$ and the precise fit $F_{\alpha=1.5913}(x)$ cannot be used for $x \gg 1$ where they decay as a power $\simeq$3.2, which is a too large number to reproduce the observations.

The universal density profile $\rho(r)/\rho(0)$ is obtained theoretically in the diluted Boltzmann regime. In such regime the density profile decreases for large $x \gg 1$ as $\sim 1/x^2$. More precisely, we find the asymptotic behavior

$$F(x) \overset{x\gg 1}{=} F_{\rm asy}(x) \equiv \frac{0.151869}{x^2}\left[1 + \mathcal{O}\left(\frac{1}{\sqrt{x}}\right)\right]. \qquad (3.2)$$

We plot in Fig. 5 $F(x)$ and its asymptotic behavior $F_{\rm asy}(x)$ vs. x. We see that $F_{\rm asy}(x)$ becomes a very good approximation to $F(x)$ for $x \gtrsim 3$. When $F(x)$ behaves as $\sim 1/x^2$ the circular velocity for these theoretical density profiles becomes constant as shown in [40].

For galaxy masses $\hat{M}_h < 10^5\ M_\odot$, near the quantum degenerate regime, the normalized density profiles $\rho(r)/\rho(0)$ are not anymore universal and depend on the galaxy mass.

As we can see in Fig. 4 the density profile shape changes fast when the galaxy mass decreases only by a factor seven from $\hat{M}_h = 1.4 \times 10^5\ M_\odot$ to the minimal galaxy mass $\hat{M}_{h,\rm min} = 3.10 \times 10^4\ M_\odot$. In this narrow range of galaxy masses the density profiles shrink from the universal profile till the degenerate profile as shown in Fig. 4. Namely, these dwarf galaxies are more compact than the larger diluted galaxies.

We display in Fig. 6 the normalized velocity dispersion profiles $\sigma^2(r)/\sigma^2(0)$ as functions of $x = r/r_h$. Again,

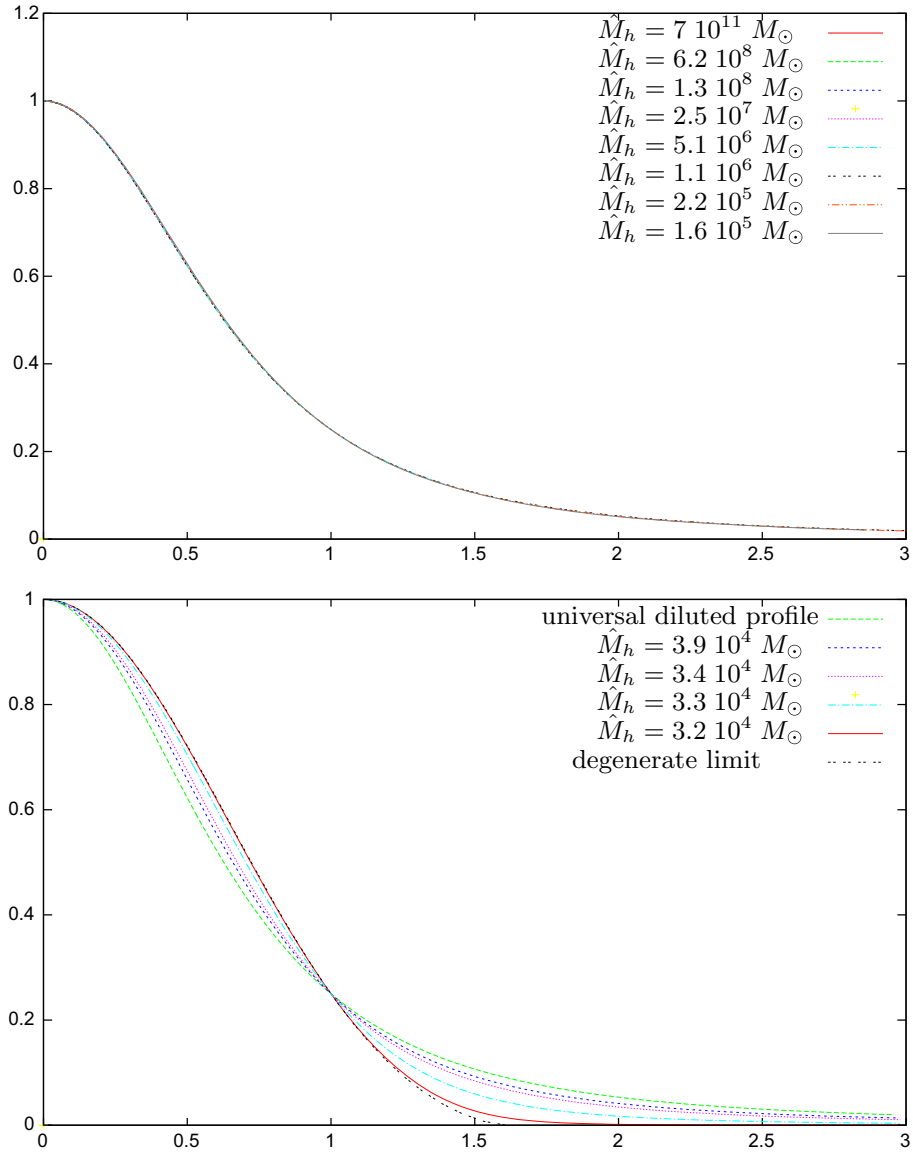

Fig. 4 Normalized density profiles $\rho(r)/\rho(0)$ as functions of r/r_h. We display in the *upper panel* the profiles for galaxy masses in the diluted regime $1.4 \times 10^5\ M_\odot < \hat{M}_h < 7.5 \times 10^{11}\ M_\odot,\ -1.5 > \nu_0 > -20.78$, which **all** provide the **same universal** density profile. We display in the *lower panel* the profiles for galaxy masses $M_h^{\min} = 30{,}999\ (2\,\mathrm{keV}/m)^{\frac{16}{5}}\ M_\odot \leq \hat{M}_h < 3.9 \times 10^4\ M_\odot,\ 1 < \nu_0 < \infty$, which are near the quantum degenerate regime and exhibit shrinking density profiles for decreasing galaxy mass. For comparison, we also plot in the *lower panel* the universal profile in the diluted regime

we see that these profiles are **universal and constant**, i.e. independent of the galaxy mass in the diluted regime for $\hat{M}_h > 2.3 \times 10^6\ M_\odot,\ \nu_0 < -5,\ T_0 > 0.017$ K. The constancy of $\sigma^2(r) = \sigma^2(0)$ in the diluted regime implies that the equation of state is that of a perfect but inhomogeneous WDM gas. Indeed, from Eq. (2.48)

$$\sigma^2(r) = \sigma^2(0) = \frac{T_0}{m}, \tag{3.3}$$

and Eq. (2.6) implies for the WDM diluted galaxies the perfect gas equation of state (4.3) where both the pressure $P(r)$ and the density $\rho(r)$ depend on the coordinates.

For smaller galaxy masses $1.6 \times 10^6\ M_\odot > \hat{M}_h > \hat{M}_{h,\min}$, the velocity profiles do depend on r and yield decreasing velocity dispersions for decreasing galaxy masses. Namely, the deviation from the universal curves appears for $\hat{M}_h < 10^6\ M_\odot$ and we see that it precisely arises from the quantum fermionic effects which become important in such range of galaxy masses.

4 The equation of state of WDM galaxies: classical diluted and compact quantum regimes

The WDM galaxy equation of state is by definition the functional relation between the pressure P and the density ρ.

From Eqs. (2.17) and (2.18) we obtain separately P and ρ at a point r as

$$\rho = \frac{m^{\frac{5}{2}}}{3\pi^2\hbar^3}\ (2\,T_0)^{\frac{3}{2}}\ I_2(\nu), \quad P = \frac{m^{\frac{3}{2}}}{15\,\pi^2\,\hbar^3}\ (2\,T_0)^{\frac{5}{2}}\ I_4(\nu). \tag{4.1}$$

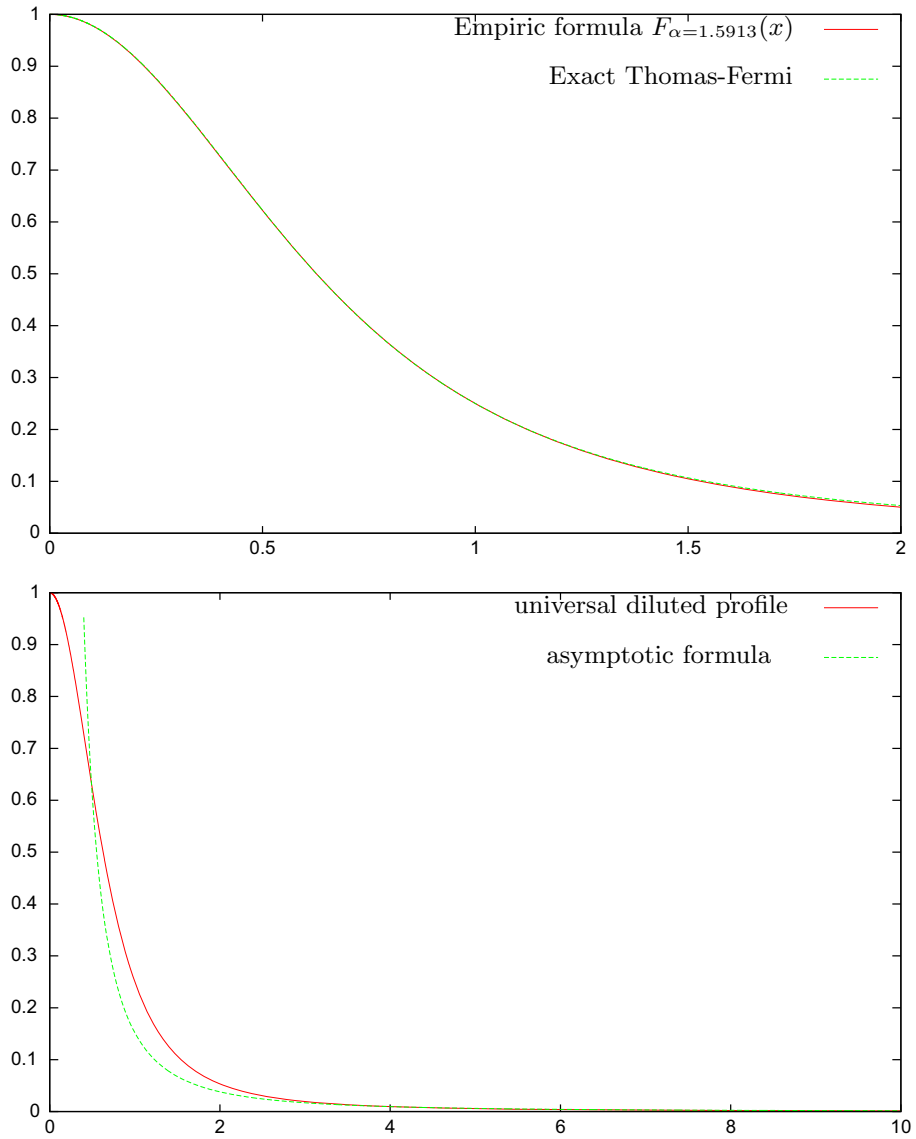

Fig. 5 *Upper panel* the universal density profile $\rho(r)/\rho(0)$ obtained from the Thomas–Fermi equations plotted versus $x = \frac{r}{r_h}$ and its fitting formula (3.1) for the best fit value $\alpha = 1.5913$. *Lower panel* the universal density profile $F(x)$ obtained from the Thomas–Fermi equations versus $x = r/r_h$ and its asymptotic form $F_{asy}(x)$ given by Eq. (3.2) versus $x = r/r_h$. For $x \gtrsim 3$, $F_{asy}(x)$ becomes a very good approximation to $F(x)$

These equations express parametrically, through the parameter ν, the pressure P as a function of the density ρ and therefore provide the WDM galaxy equation of state.

For fermionic WDM in thermal equilibrium $I_2(\nu)$ and $I_4(\nu)$ are given as integrals of the Fermi–Dirac distribution function in Eq. (2.15). For WDM out of thermal equilibrium Eq. (4.1) is always valid but $I_2(\nu)$ and $I_4(\nu)$ should be expressed as integrals of the corresponding out of equilibrium distribution function. In the out of equilibrium case T_0 is just the characteristic scale in the out of equilibrium distribution function $f_{\rm out}(E) = \Psi_{\rm out}(E/T_0)$. For the relevant galaxy physical magnitudes, the Fermi–Dirac distribution gives similar results to the out of equilibrium distribution functions [31].

In the two WDM galaxy regimes, classical diluted regime, and degenerate quantum regime, we can eliminate ν in Eq. (4.1) and obtain P as a function of ρ in close form. Let us take the ratios P/ρ and $P/\rho^{\frac{5}{3}}$ in Eq. (4.1):

$$\frac{P}{\rho} = \frac{2}{5}\,\frac{T_0}{m}\,\frac{I_4(\nu)}{I_2(\nu)}, \quad \frac{P}{\rho^{\frac{5}{3}}} = \frac{\hbar^2}{5}\left(\frac{3\pi^2}{m^4}\right)^{\frac{2}{3}}\frac{I_4(\nu)}{I_2^{\frac{5}{3}}(\nu)}. \tag{4.2}$$

In the diluted limit $\nu \ll -1$ we have

$$\frac{I_4(\nu)}{I_2(\nu)} \overset{\nu\ll -1}{=} \frac{5}{2},$$

and therefore we obtain for WDM in the diluted limit the local perfect gas equation of state:

$$P(r) = \frac{T_0}{m}\,\rho(r), \quad \text{WDM diluted galaxies.} \tag{4.3}$$

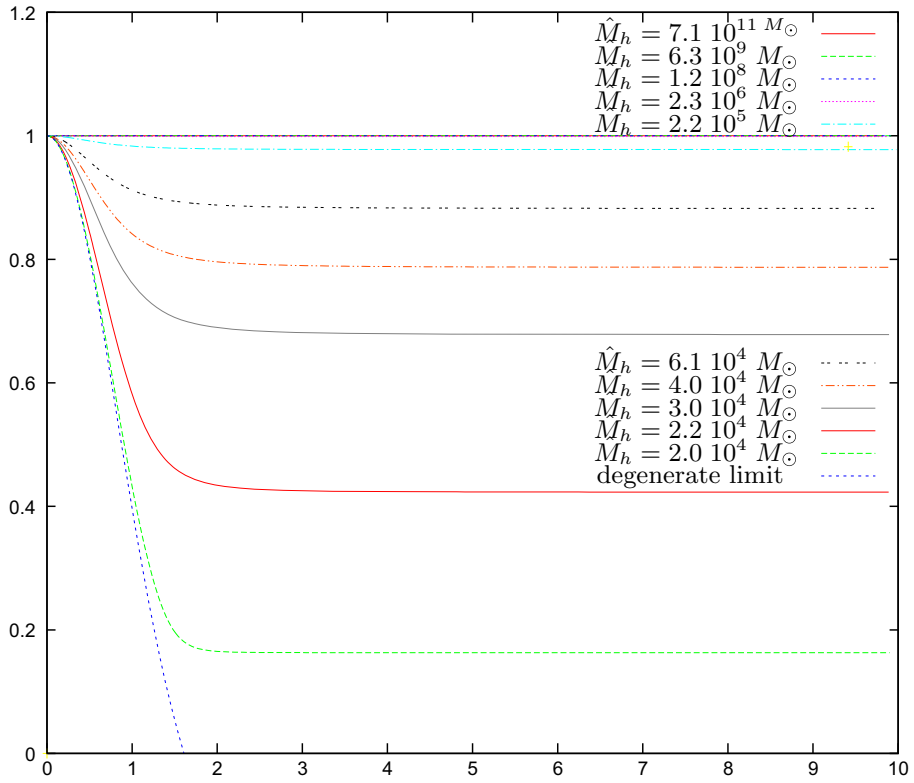

Fig. 6 Normalized velocity dispersion profiles $\sigma^2(r)/\sigma^2(0)$ as functions of $x = r/r_h$. All velocity profiles in the diluted regime for galaxy masses $\hat{M}_h > 2.3 \times 10^6\ M_\odot,\ \nu_0 < -5$ fall into the same **constant universal** profile corresponding to a perfect but inhomogeneous self-gravitating WDM gas describing large and diluted galaxies. The velocity profiles for smaller galaxy masses $1.6 \times 10^6\ M_\odot > \hat{M}_h > \hat{M}_{h,\min} = 3.10 \times 10^4\ M_\odot$ do depend on x and yield decreasing velocity dispersions for decreasing galaxy masses, accounting for the quantum fermionic effects which become important in this range of galaxy masses (WDM compact dwarf galaxies)

The local perfect WDM gas equation of state (4.3) is precisely the equation of state of the Boltzmann self-gravitating gas [51].

In the degenerate limit $\nu \gg 1$ we have

$$\frac{I_4(\nu)}{I_2^{\frac{5}{3}}(\nu)} \overset{\nu\gg 1}{=} 1$$

and therefore $P/\rho^{\frac{5}{3}}$ in Eq. (4.2) becomes the degenerate fermionic equation of state at $T_0 = 0$,

$$P = \frac{\hbar^2}{5}\left(\frac{3\pi^2}{m^4}\right)^{\frac{2}{3}} \rho^{\frac{5}{3}}, \quad \text{WDM degenerate quantum limit.} \tag{4.4}$$

Making explicit the dimensions, the WDM galaxy equation of state (4.1) becomes

$$\rho = 4.68591 \times 10^4 \left(\frac{T_0}{\mathrm{K}}\right)^{\frac{3}{2}} I_2(\nu) \left(\frac{m}{2\,\mathrm{keV}}\right)^{\frac{5}{2}} \frac{M_\odot}{\mathrm{pc}^3},$$
$$P = 0.807603\ 10^{-3} \left(\frac{T_0}{\mathrm{K}}\right)^{\frac{5}{2}} I_4(\nu) \left(\frac{m}{2\,\mathrm{keV}}\right)^{\frac{3}{2}} \frac{M_\odot}{\mathrm{pc}^3}. \tag{4.5}$$

The galaxies being non-relativistic systems, P turns out to be much smaller than ρ when both are written in the same units where the speed of light is taken to be unit.

It is useful to introduce the rescaled dimensionless variables

$$\bar{\rho} \equiv \left(\frac{2\,\mathrm{keV}}{m}\right)^{\frac{5}{2}} \frac{\mathrm{pc}^3}{M_\odot} \rho = 4.68591\ 10^4 \left(\frac{T_0}{\mathrm{K}}\right)^{\frac{3}{2}} I_2(\nu)$$
$$\bar{P} \equiv \left(\frac{2\,\mathrm{keV}}{m}\right)^{\frac{3}{2}} \frac{\mathrm{pc}^3}{M_\odot} P = 0.807603\ 10^{-3} \left(\frac{T_0}{\mathrm{K}}\right)^{\frac{5}{2}} I_4(\nu). \tag{4.6}$$

We plot in Fig. 7 the common (base 10) logarithm of $\bar{P}$ vs. the common logarithm of $\bar{\rho}$ for different values of T_0. For small density and for growing effective temperature, the self-gravitating ideal WDM gas behavior Eq. (4.3) of the diluted regime is obtained. On the contrary, for large density and for decreasing temperature the fermionic quantum behavior close to the degenerate state Eq. (4.4) shows up. That is, the straight lines with unit slope in Fig. 7 describe the perfect WDM gas behavior Eq. (4.3), while the steeper straight lines with slope 5/3 describe the degenerate quantum behavior Eq. (4.4). We see that the diluted classical and degenerate regimes are interpolated smoothly by the quantum behavior. For increasing T_0 the curves in Fig. 7 move up. The larger T_0 is, the larger is the value of the density $\bar{\rho}$ where the quantum behavior is attained.

We plot in Fig. 8 the pressure normalized to its value at the origin as a function of the density normalized to its value at the origin according to Eq. (4.1):

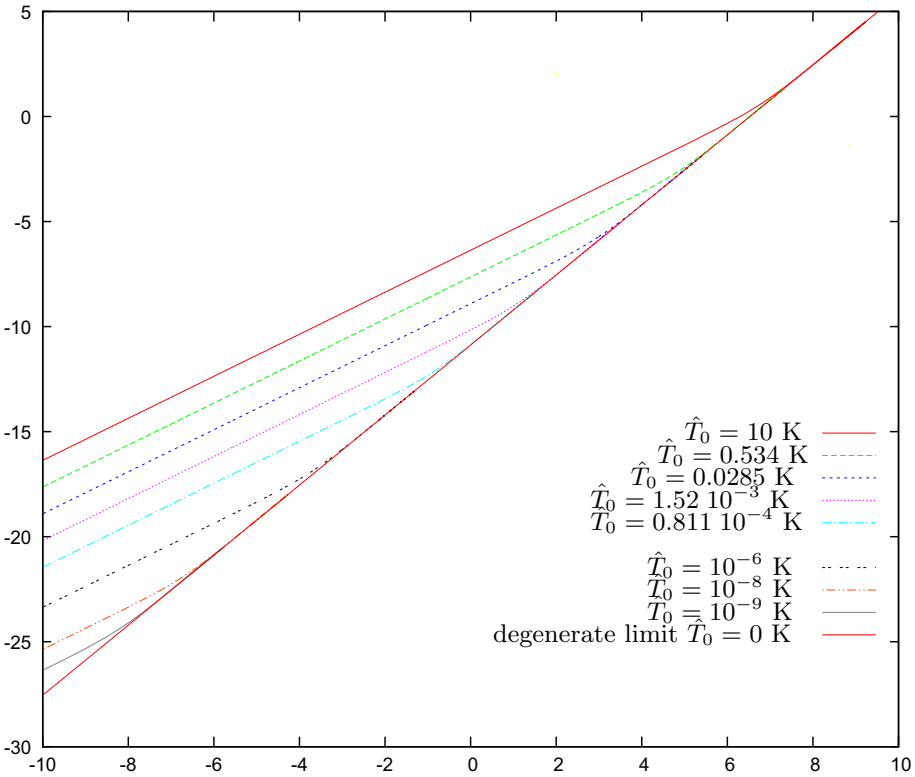

Fig. 7 The equation of state of WDM galaxies. Logarithmic plot [in common (base 10) logarithm] of the galaxy pressure $\bar{P}$ versus the density $\bar{\rho}$ as defined by Eq. (4.6) for different values of the effective temperature T_0. For small density and growing T_0, the self-gravitating ideal WDM gas behavior is obtained exhibiting straight lines with unit slope; this describes the physical state of large diluted galaxies $\hat{M}_h > 2.3 \times 10^6\ M_\odot,\ \nu_0 < -5,\ T_0 > 0.017$ K. For large density and decreasing temperature the fermionic quantum behavior close to the degenerate state equation (4.4) shows up as the steeper straight lines with slope approaching 5/3. In particular, the degenerate $T_0 = 0$ state exhibits the slope 5/3 for all densities. The diluted classical regime and the degenerate regime are interpolated smoothly by the quantum behavior corresponding to compact dwarf galaxies with $1.6 \times 10^6\ M_\odot > \hat{M}_h \geq \hat{M}_{h,\min} = 3.10 \times 10^4\ M_\odot,\ \nu_0 > -4,\ T_0 < 0.011$ K. For increasing T_0 the curves move up. The larger is T_0, the larger is the value of the density $\bar{\rho}$ where the quantum behavior is attained

$$\frac{P}{P_0} = \frac{I_4(\nu)}{I_4(\nu_0)} \quad \text{vs.} \quad \frac{\rho}{\rho_0} = \frac{I_2(\nu)}{I_2(\nu_0)}. \tag{4.7}$$

The diluted and degenerate gas behaviors Eqs. (4.3) and (4.4) of WDM galaxies are explicitly seen in Fig. 8. The diluted perfect gas behavior appears for galaxy masses $\hat{M}_h > 2.3 \times 10^6\ M_\odot,\ \nu_0 < -5,\ T_0 > 0.017$ K. The degenerate gas behavior shows up for the minimal mass galaxy $\hat{M}_{h,\min} = 3.10 \times 10^4\ M_\odot,\ T_0 = 0$.

Besides the two limiting regimes, diluted and degenerate, we see from Fig. 8 that the equation of state **does depend** on the galaxy mass for galaxy masses in the range $1.6 \times 10^6\ M_\odot > \hat{M}_h \geq \hat{M}_{h,\min},\ \nu_0 > -4,\ T_0 < 0.011$ K. This is a quantum regime, close to but not at, the degenerate limit. The equation of state in this quantum regime is steeper than in the degenerate limit.

We find that WDM galaxies exhibit two regimes: classical diluted and quantum compact (close to degenerate). WDM galaxies are diluted for $\hat{M}_h > 2.3 \times 10^6\ M_\odot,\ \nu_0 < -5,\ T_0 > 0.017$ K and they are quantum and compact for $1.6 \times 10^6\ M_\odot > \hat{M}_h \geq \hat{M}_{h,\min},\ \nu_0 > -4,\ T_0 < 0.011$ K. The degenerate limit $T_0 = 0$ corresponds to the extreme quantum situation yielding a minimal galaxy size $\hat{r}_{h,\min}$ and mass $\hat{M}_{h,\min}$ given by Eq. (2.49). The equation of state covering all regimes is given by Eq. (4.1).

We therefore find an explanation for the universal density profiles and universal velocity profiles in diluted galaxies ($\hat{M}_h \gtrsim 10^6\ M_\odot$): these **universal properties** can be traced back to the perfect gas behavior of the self-gravitating WDM gas summarized by the WDM equation of state (4.3). Notice that all these universal theoretical profiles well reproduce the observations for $r \lesssim r_h$ [40].

For small galaxy masses, $10^6\ M_\odot \gtrsim \hat{M}_h \geq \hat{M}_{h,\min} = 3.10 \times 10^4\ M_\odot$, which correspond to chemical potentials at the origin $\nu_0 \gtrsim -5$ and effective temperatures $T_0 \lesssim 0.017$ K, the equation of state is galaxy mass dependent (see Fig. 8) and the profiles are not anymore universal. These properties account for the quantum physics of the self-gravitating WDM fermions in the compact case close to the degenerate state.

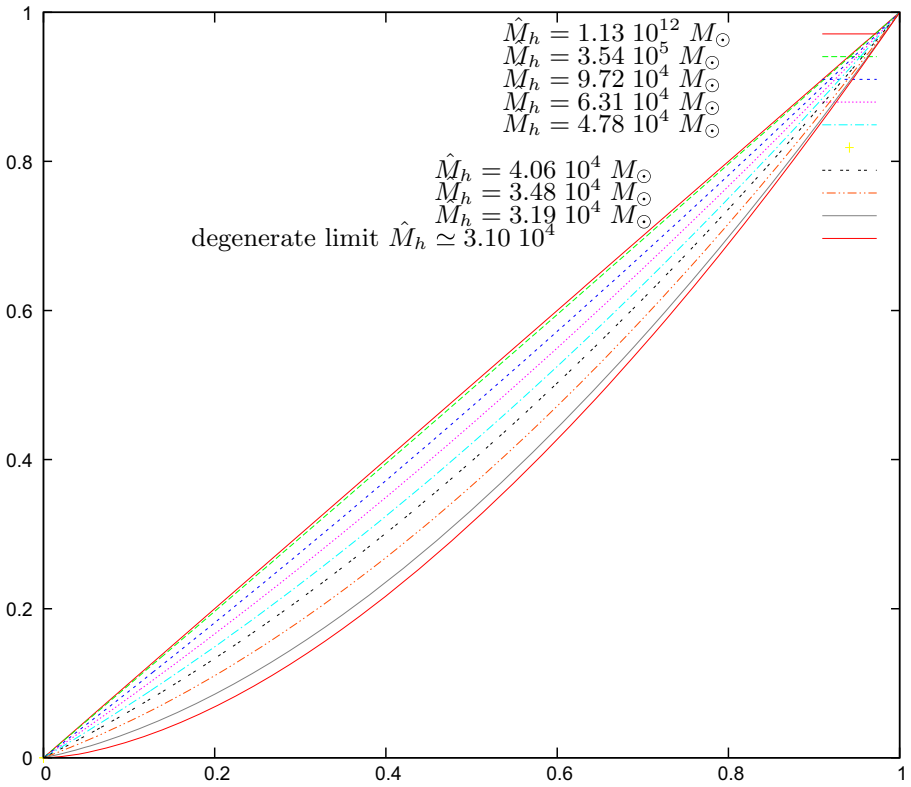

Fig. 8 The galaxy pressure P/P_0 versus the density ρ/ρ_0, where P_0 and ρ_0 are the pressure and the density at the origin, respectively defined by Eq. (4.7). We see the WDM ideal gas behavior (unit slope) in the diluted regime, that is, for galaxy masses $\hat{M}_h > 2.3 \times 10^6\ M_\odot,\ \nu_0 < -5,\ T_0 > 0.017$ K. For smaller galaxy masses, $1.6 \times 10^6\ M_\odot > \hat{M}_h \geq \hat{M}_{h,\min} = 3.10 \times 10^4\ M_\odot,\ \nu_0 > -4$, the equation of state depends on the galaxy mass and becomes steeper corresponding to the quantum fermionic regime of dwarf galaxies. In the degenerate limit $\nu_0 = \infty$ we obtain a 5/3 slope straight line. We see that the diluted and degenerate regimes are interpolated smoothly by the quantum behavior

Indeed, it will be extremely interesting to dispose of observations which could check these quantum effects in dwarf galaxies.

A useful empirical fit of the exact equation of state follows by expressing the pressure given by (4.1),

$$P = \frac{m^{\frac{3}{2}}\ (2\ T_0)^{\frac{5}{2}}}{15\,\pi^2\,\hbar^3}\ \tilde{P} \quad \text{where} \quad \tilde{P} \equiv I_4(\nu), \tag{4.8}$$

as a function of

$$\tilde{\rho} \equiv \frac{3\,\pi^2\,\hbar^3}{m^{\frac{5}{2}}\ (2\ T_0)^{\frac{3}{2}}}\ \rho = I_2(\nu). \tag{4.9}$$

We represent $\tilde{P}$ as a function $\tilde{\rho}$ through the simple function

$$\tilde{P} = \left(1 + \frac{3}{2}\ e^{-\beta_1\ \tilde{\rho}}\right)\ \tilde{\rho}^{\frac{1}{3}(5\ -\ 2\ e^{-\beta_2\ \tilde{\rho}})}, \tag{4.10}$$

which exactly fulfills the diluted and degenerate limiting behaviors (4.3) and (4.4), respectively. Equation (4.10) best fits the exact values of $\tilde{P}$ as a function $\tilde{\rho}$ obtained by solving the Thomas–Fermi equation (2.3) for

$$\beta_1 = 0.047098, \quad \beta_2 = 0.064492. \tag{4.11}$$

In summary, we represent the equation of state as

$$P = \frac{m^{\frac{3}{2}}\ (2\ T_0)^{\frac{5}{2}}}{15\,\pi^2\,\hbar^3}\ \left(1 + \frac{3}{2}\ e^{-\beta_1\ \tilde{\rho}}\right)\ \tilde{\rho}^{\frac{1}{3}(5\ -\ 2\ e^{-\beta_2\ \tilde{\rho}})}$$

where $\tilde{\rho}$ is expressed in terms of ρ by Eq. (4.9). We plot in Fig. 9 $\tilde{P}$ vs. $\tilde{\rho}$ obtained by solving the Thomas–Fermi equation (2.3) and the empirical fit equation (4.10). One can see that the fit turns out to be excellent.

5 The dependence on the WDM particle mass in the diluted and quantum regimes

In the diluted limit the velocity dispersion is constant $\sigma^2(r) = \sigma^2(0)$, and Eq. (2.11) and Eq. (3.3) lead to

$$\frac{\mathrm{d}^2\mu}{\mathrm{d}r^2} + \frac{2}{r}\ \frac{\mathrm{d}\mu}{\mathrm{d}r} = -4\pi\ G\ m\ \rho(r) \tag{5.1}$$

$$\rho(r) = \frac{1}{4}\ \left(\frac{2\ T_0}{\pi\ m}\right)^{\frac{3}{2}}\ m^4\ \exp\left[\frac{\mu(r)}{T_0}\right]. \tag{5.2}$$

In this diluted limit, the Thomas–Fermi equations (2.3) become the equations for a self-gravitating Boltzmann gas in thermal equilibrium.

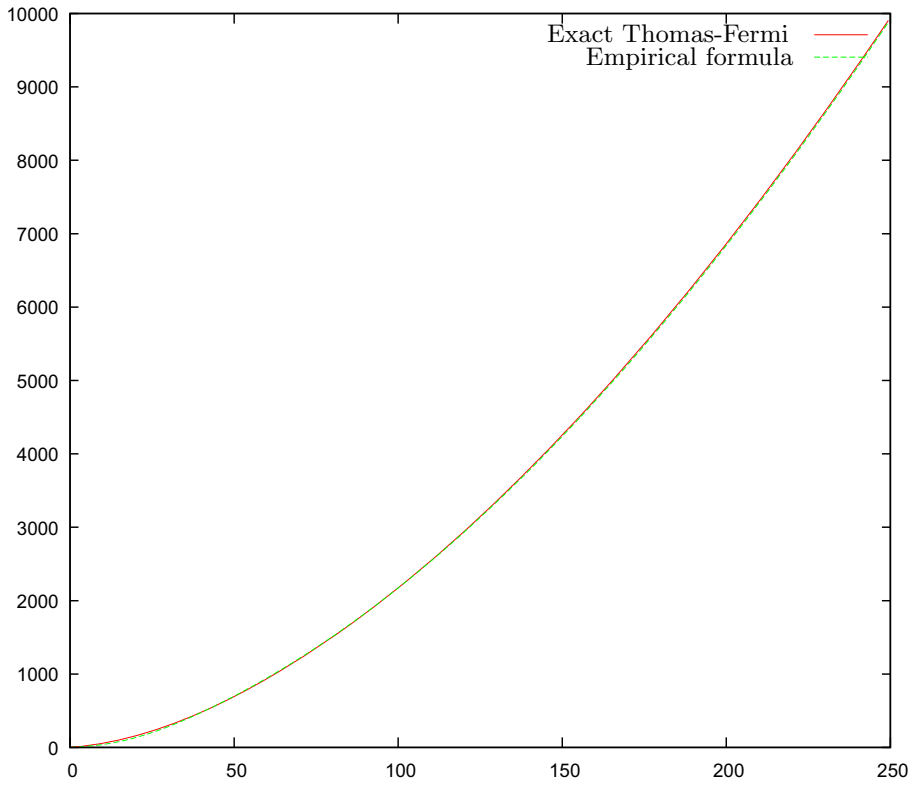

Fig. 9 The equation of state $\tilde{P}$ versus $\tilde{\rho}$ obtained by solving the Thomas–Fermi equation (2.3) and the empirical fit equations (4.9), (4.10). The exact equation of state and the fitting formula cannot be distinguished at this resolution

Equation (5.2) combined with the chemical potential equation (2.1) becomes the barotropic equation,

$$\rho(r) = \rho_0 \, \mathrm{e}^{-\frac{m}{T_0}\,[\phi(r)-\phi(0)]}.$$

It is instructive to discuss from Eq. (5.1) the dependence on the mass m of the WDM particle.

In the diluted regime, T_0 and $\mu(r)$ depend on m, while the other magnitudes as $\rho(r)$, $M(r)$, $\sigma^2(r)$, $P(r)$, $Q(r)$, and $\phi(r)$ do not depend on m. This means that a change in m, namely

$$m \Rightarrow m',$$

must leave Eq. (5.1) invariant, which implies

$$\frac{T_0}{m} = \text{invariant}, \quad m^4 \, \exp\left[\frac{\mu(r)}{T_0}\right] = \text{invariant}.$$

That is,

$$\begin{aligned} T_0(m') &= \frac{m'}{m}\, T_0(m), \quad \mu(m', r) \\ &= \frac{m'}{m}\left[\mu(m, r) + 4\, T_0(m)\, \ln\left(\frac{m}{m'}\right)\right]. \end{aligned} \tag{5.3}$$

A change in the WDM particle mass m implies that the temperature T_0 and the chemical potential $\mu(r)$ transform as given by Eq. (5.3). These transformations leave the Boltzmann gas equations (5.1) and (5.2) invariant.

Under changes of m the dimensionless variables ξ and $\nu(\xi)$ transform as

$$\begin{aligned} &m \Rightarrow m', \quad \xi' = \xi \left(\frac{m'}{m}\right)^2, \\ &\nu(\xi', m') = \nu(\xi, m) + 4\, \ln\left(\frac{m}{m'}\right). \end{aligned} \tag{5.4}$$

We see that all the diluted regime relations Eqs. (2.37)–(2.47) are invariant under the change $m \Rightarrow m'$ implemented through Eqs. (5.3), (5.4).

Indeed, this invariance is restricted to the diluted regime ($\hat{M}_h \gtrsim 10^6\, M_\odot$).

For galaxy masses $\hat{M}_h < 10^5\, M_\odot$, namely in the **quantum regime of compact dwarf galaxies**, all physical quantities **do depend** on the DM particle mass m as explicitly displayed in Eqs. (2.17)–(2.35). It is precisely this dependence on m that leads to the lower bound $m > 1.91$ keV from the minimum observed galaxy mass [31]. Moreover, for $m > 2$ keV, an overabundance of small structures appears as solution of the Thomas–Fermi equations, which do not have an observed counterpart. Therefore, m between 2 and 3 keV is singled out as the most plausible value [31].

In summary, we see the power of the WDM Thomas–Fermi approach to describe the structure and the physical state of galaxies in a clear way and in very good agreement with observations.

Funded by SCOAP[3].

References

1. Cosmic Frontier, H.J. de Vega, N.G. Sanchez, arXiv:1304.0759
2. Highlights and Conclusions of the Chalonge 16th Paris Cosmology Colloquium 2012. arXiv:1307.1847
3. Highlights and Conclusions of the Chalonge Meudon Workshop 2012. arXiv:1305.7452
4. H.J. de Vega, N.G. Sánchez, Mon. Not. R. Astron. Soc. **404**, 885 (2010)
5. H.J. de Vega, P. Salucci, N.G. Sanchez, New Astron. **17**, 653 (2012)
6. N. Menci, F. Fiore, A. Lamastra, ApJ **766**, 110 (2013)
7. A.M. Nierenberg et al., ApJ **772**, 146 (2013)
8. F. Pacucci et al., MNRAS Lett. **435**, L53 (2013)
9. S. Shao et al., MNRAS **430**, 2346 (2013)
10. C.R. Watson, Z. Li, N. Polley, JCAP **03**, 018 (2012)
11. D. Anderhalden et al., JCAP **03**, 014 (2013)
12. P. Colín, O. Valenzuela, V. Avila-Reese, ApJ **542**, 622 (2000)
13. L. Gao, T. Theuns, Science **317**, 1527 (2007)
14. M.R. Lovell et al., MNRAS **420**, 2318 (2012)
15. M.R. Lovell et al., Mon. Not. R. Astron. Soc. **439**, 300 (2014)
16. E. Papastergis et al., ApJ **739**, 38 (2011)
17. J. Sommer-Larsen, A. Dolgov, ApJ **551**, 608 (2001)
18. A.V. Tikhonov et al., MNRAS **399**, 1611 (2009)
19. J. Zavala et al., ApJ **700**, 1779 (2009)
20. G. Gilmore et al., ApJ **663**, 948 (2007)
21. M. Walker, J. Peñarrubia, ApJ **742**, 20 (2011)
22. R.F.G. Wyse, G. Gilmore, IAU Symposium, vol. 244, pp. 44–52 (2007). arXiv:0708.1492
23. J. van Eymeren et al., A & A **505**, 1–20 (2009)
24. W.J.G. de Blok, Adv. Astron. **2010**, 1–15 (2010). arXiv:0910.3538
25. P. Salucci, Ch. Frigerio Martins, EAS Publ. Ser. **36**, 133–140 (2009). arXiv:0902.1703
26. V. Avila-Reese et al., ApJ **559**, 516 (2001)
27. P. Colín, O. Valenzuela, V. Avila-Reese, ApJ **673**, 203 (2008)
28. A. Macciò, S. Paduroiu, D. Anderhalden, A. Schneider, B. Moore, MNRAS **424**, 1105 (2012)
29. J. Viñas, E. Salvador-Solé, A. Manrique, MNRAS **424**, L6 (2012)
30. C. Destri, H.J. de Vega, N.G. Sanchez, New Astron. **22**, 39 (2013)
31. C. Destri, H.J. de Vega, N.G. Sanchez, Astropart. Phys. **46**, 14 (2013)
32. L.D. Landau, E.M. Lifshits, *Statistical Mechanics* (Elsevier, Oxford, 1980)
33. S.L. Shapiro, S.A. Teukolsky, *Black Holes, White Dwarfs, and Neutron Stars* (Wiley, Weinheim, 2004)
34. F. Munyaneza, P.L. Biermann, A & A **458**, L9 (2006)
35. P.H. Chavanis, Phys. Rev. E **65**, 056123 (2002)
36. P.H. Chavanis, Int. J. Mod. Phys. B **20**, 3113 (2006)
37. See, for example G. Gallavotti, *Statistical Mechanics: A Short Treatise* (Springer, Berlin, 1999)
38. F. Donato et al., MNRAS **397**, 1169 (2009)
39. M. Spano et al., MNRAS **383**, 297 (2008)
40. H.J. de Vega, P. Salucci, N.G. Sanchez, Mon. Not. R. Astron. Soc. **442**, 2717 (2014)
41. J. Binney, S. Tremaine, *Galactic Dynamics*, 2nd edn. (Princeton University Press, Princeton, 2008)
42. J. Kormendy, K.C. Freeman, IAU Symposium, Sydney, vol. 220, p. 377 (2004). arXiv:astro-ph/0407321
43. A.W. McConnachie, AJ **144**, 4 (2012)
44. P. Salucci et al., MNRAS **378**, 41 (2007)
45. J.D. Simon, M. Geha, ApJ **670**, 313 (2007). (and references therein)
46. J.D. Simon et al., ApJ **733**, 46 (2011). (and references therein)
47. J. Wolf et al., MNRAS **406**, 1220 (2010). (and references therein)
48. J.P. Brodie et al., AJ **142**, 199 (2011)
49. G.D. Martinez et al., ApJ **738**, 55 (2011)
50. B. Willman, J. Strader, AJ **144**, 76 (2012)
51. H.J. de Vega, N.G. Sánchez, Nucl. Phys. B **625**, 409, 460 (2002)